



Destructive and nondestructive characteristics of solidified reservoir sediments incorporating microstructural analyses

Pitthaya Jamsawang¹ · Hatairat Poorahong² · Pornkasem Jongpradist³ · Suched Likitlersuang⁴ · Salisa Chaiyaput⁵

Received: 7 June 2021 / Accepted: 19 June 2022 / Published online: 29 July 2022
© Springer-Verlag GmbH Germany, part of Springer Nature 2022

Abstract

Reservoir sediments create a range of severe problems for hydropower dams. Although reservoir sediments can be excavated, nonetheless, sizeable dumping lands for such excavated sediments are unavailable at this time. This paper presents an experimental investigation of the destructive and nondestructive properties and microstructural characteristics of reservoir sediments solidified with fly ash–cement blend for reuse as construction materials. The obtained natural sediment was classified as well-graded sand with silt. The destructive experiments comprised unconfined compression, indirect tension, California bearing ratio, resilient modulus, and durability against wet–dry cycle tests, while the nondestructive experiments included a free–free resonance test. Microstructural investigations consisting of X-ray diffraction, thermogravimetric analysis, scanning electron microscopy, and energy-dispersive X-ray spectrometry were performed to verify the macroscale test results. The results showed that fly ash–cement blend exhibited increased strength values on the order of 2 to 9 times that of unsolidified sediments. Using fly ash-blended cement was more effective than using sole cement or sole fly ash, and mixtures with 10% fly ash delivered the best strength and modulus values. Various functional empirical correlations were proposed. Utilizing six wet–dry cycles is acceptable because the strength of the samples subjected to the six wet–dry cycles was lower than the given value. The results of the peak intensities of calcium silicate hydrate, mass losses, calcium contents, and scanning electron microscopy images derived from the microstructural investigations confirmed the macroscale test results.

Keywords Destructive test · Durability · Fly ash-blended cement · Microstructure · Nondestructive test · Reservoir sediment

Introduction

Reservoir sediments represent an amalgamation of various noncompacted soil particles, including gravel, sand, silt, and clay, induced by soil erosion and rock weathering processes

(Dubois et al. 2011). Reservoir sediments develop from the transportation and deposition processes of natural sediments in reservoirs contained by dams (Banoune et al. 2016; Chan 2016; Dang et al. 2013; Furlan et al. 2018; Silitonga et al. 2009, 2010; Wang et al. 2012, 2013, 2018; Zeng et al. 2017;

✉ Pitthaya Jamsawang
pitthaya.j@eng.kmutnb.ac.th

Hatairat Poorahong
s6001081914512@email.kmutnb.ac.th

Pornkasem Jongpradist
pornkasem.jon@kmutt.ac.th

Suched Likitlersuang
fceslk@eng.chula.ac.th

Salisa Chaiyaput
salisa.ch@kmitl.ac.th

¹ Soil Engineering Research Center, Department of Civil Engineering, King Mongkut's University of Technology North Bangkok, Bangkok 10800, Thailand

² Department of Civil Engineering, Bangkokthonburi University, Bangkok 10170, Thailand

³ Department of Civil Engineering, Faculty of Engineering, King Mongkut's University of Technology Thonburi, Bangkok 10140, Thailand

⁴ Centre of Excellence in Geotechnical and Geoenvironmental Engineering, Department of Civil Engineering, Faculty of Engineering, Chulalongkorn University, Bangkok 10330, Thailand

⁵ Department of Civil Engineering, School of Engineering, King Mongkut's Institute of Technology Ladkrabang, Bangkok 10520, Thailand

Zentar et al. 2021; Zhang et al. 2018). More than twenty hydropower dams operated by the Department of Alternative Energy Development and Efficiency (DAEDE) under the Ministry of Energy of Thailand have faced large amounts of excessive reservoir sediments behind their dams. Such excessive sediments generate many severe problems, including reducing the storage capacity, discharge ability, flood control capability, and electric energy production efficiency of the dams. Furthermore, reservoir sediments also affect dam safety, such as leading to excessive loads on the dam body and dam gates, damaging mechanical equipment, and creating a wide range of environmental impacts. Reservoir sediments are regularly excavated to maintain dam abilities and safety. Therefore, the excavated reservoir sediment is characterized as waste and, as such, is generally discarded in the sea or land dumps (Kamali et al. 2008).

The DAEDE arranges to excavate such excessive reservoir sediments. However, the sizeable dumping land areas needed to support such excavated sediments are unavailable because most of the area around such reservoirs tends to be agricultural and farming regions. Thus, the DAEDE decided to reuse these wastes as construction and building materials, such as compressed earth blocks and road materials, to benefit the community within the vicinity. The first pilot project was the reuse of reservoir sediments in the Huai Mae Phong hydropower dam, located in Phayao Province, Thailand (Fig. 1a and b). However, the reuse of reservoir sediments without treatment would not feasibly deliver appropriate standard construction materials. Solidification of the excavated reservoir sediments using stabilizers that are locally available in Thailand, such as cement and fly ash, is introduced in regard to cost-effectiveness, construction practice, and waste management.

Solidification with cement alone is the most conventional method for enhancing the strengths and moduli of

problematic soil properties in various applications (Güllü et al. 2017; Horpibulsuk et al. 2010, 2011a, b; Jamsawang et al. 2017a, b; Kamali et al. 2008; Mohammadinia et al. 2015; Voottipruex and Jamsawang 2014; Yoobanpot et al. 2017; Chompoorat et al. 2019). Class C fly ash is a famous byproduct derived from the combustion process of lignite coal in power plants (Jamsawang et al. 2017a, b; Yoobanpot et al. 2017). Class C fly ash is considered cementitious and pozzolanic because it has a suitable self-cementing property and contains active silica and alumina (Jamsawang et al. 2017a, b; Yoobanpot et al. 2017). The fly ash production rate is much higher than its reuse rate. Therefore, recycling of fly ash as road materials in civil engineering applications provides notable environmental advantages, such as relieving air contaminants and reducing water pollution (Banoune et al. 2016; Silitonga et al. 2009; Wang et al. 2012; Zentar et al. 2021). The use of fly ash alone can increase the strength and stiffness and reduce the compressibility and swell potential of poor soils due to cation exchange, flocculation, and microfillers (Horpibulsuk et al. 2009; Silitonga et al. 2009; Tastan et al. 2011; Wang et al. 2012). An amount of 21% fly ash was found to be optimal for obtaining the best strength development with soft Bangkok clay within the active zone (Horpibulsuk et al. 2013). A sole fly ash content of 14% was sufficient to provide the same swell potential of the treated expansive clays as a sole cement content of 3%. However, the exclusive use of fly ash was not able to deliver the same strength as the use of sole cement (Voottipruex and Jamsawang 2014). The strength and modulus of the soft organic soils solidified with 10–20% fly ash were 2 to 6 times greater than those of the unsolidified sample (Horpibulsuk et al. 2009). Class C fly ash can also be blended with cement to increase the performance of the soil stabilization process by increasing



Fig. 1 **a** Location of Phayao province, Thailand, and **b** Huai Mae Phong reservoir

the reactive surface area for hydration and pozzolanic reactions (Tastan et al. 2011; Chompoorat et al. 2022).

The important destructive properties for solidified soils intended for use in construction materials include the unconfined compressive strength (q_u), indirect tensile strength (q_t), strain at failure (ϵ_f), California bear ratio (CBR), secant elastic modulus (E_{50}), and resilient modulus (M_r). In contrast, the main nondestructive characteristics comprise the shear wave (V_s) and compression wave (V_p) velocities, which can be determined by free–free resonance (FFR) tests. The FFR test is extensively employed for characterizing material properties because it is a rapid test that can be carried out on samples of various sizes (Bogas et al. 2013; Biswal et al. 2020; Moon et al. 2020; Chompoorat et al. 2021a). The dynamic moduli, including the dynamic Young's modulus (E_0), shear modulus (G_0), and dynamic Poisson's ratio (ν_0), are essential parameters for geotechnical design and predicting the behavior of soil subjected to earthquakes, explosions, and vibrations. The dynamic moduli can also be used as indirect soil parameters for general analyses in civil engineering works (Bogas et al. 2013; Biswal et al. 2020; Moon et al. 2020; Chompoorat et al. 2021a). Microstructural analyses by X-ray diffraction (XRD), thermogravimetric analysis (TGA), energy dispersive X-ray spectrometry (EDX), and scanning electron microscopy (SEM) techniques have commonly been applied for investigating the changes in microstructures of stabilized soils and sediments after the completion of destructive tests (Chan et al. 2016; Güllü et al. 2017; Kang et al. 2014; Jamsawang et al. 2017a, b; Jiang et al. 2016, 2018; Voottipruex and Jamsawang 2014; Wang et al. 2013; Zhang et al. 2018; Chompoorat et al. 2021b).

The destructive properties and corresponding microstructural characteristics of sediments solidified by either cement or fly ash alone have been studied by many researchers (Bogas et al. 2013; Dubois et al. 2011; Furlan et al. 2018; Silitonga et al. 2009; Wang et al. 2012, 2013; Zeng et al. 2017; Yoobanpot et al. 2020a, b; Zentar et al. 2021; Jamsawang et al. 2021). In contrast, few studies have

been conducted entirely on sediments solidified with fly ash–cement blend. As mentioned above, most of the previous test results were concentrated on only the q_u and E_{50} values rather than other destructive properties. Only XRD and SEM analysis results were presented to confirm the increases in the q_u and E_{50} values of the solidified sediments. Moreover, as previously mentioned, limited relevant nondestructive characteristics have been determined to investigate correlations between destructive and nondestructive properties. This study presents experimental work to evaluate various destructive and nondestructive properties of reservoir sediments solidified with fly ash–cement blend relevant to construction materials. Numerous functional correlations are provided. Several microstructural analyses are employed to investigate changes in the microstructures and support the macroscale test results.

Research methodology

Materials

The primary raw materials used in the current study included reservoir sediment, type I ordinary Portland cement, and fly ash, as shown in Fig. 2. The natural reservoir sediments were excavated with an excavator from the Huai Mae Phong Reservoir, Phayao Province, Thailand. They were then delivered to the geotechnical engineering laboratory at King Mongkut's University of Technology North Bangkok, Bangkok, Thailand. The fly ash, a byproduct of coal ash lignite, was delivered from the Mae Moh electric power plant, located in Thailand's Lampang province. SEM photos of the primary raw materials, as shown in Fig. 2, reveal that the sediments contained various particle sizes, such as coarse-grained and fine-grained particles with irregular shapes. The cement particles exhibited rough surfaces and nonuniform angular shapes, whereas the fly ash particles showed spherical shapes with uneven surfaces.

Fig. 2 Real and SEM photos of the raw materials used in this study

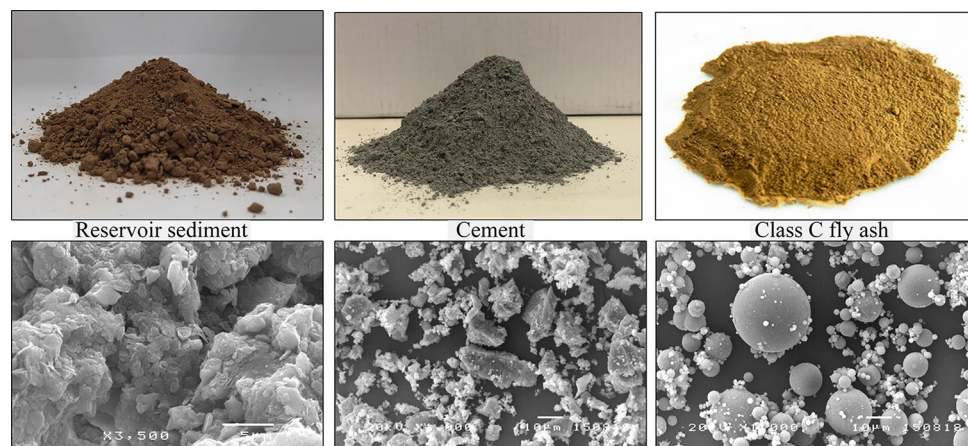


Figure 3 presents a grain size distribution curve and the geotechnical properties of the raw sediment. The raw sediment was comprised of 89% sand, 11% silt, and 4% clay contents, classified as group symbols of SW-SM and group names of well-graded sand with silt following the Unified Soil Classification System (Table 1). The maximum dry unit weight was 16.5 kN/m^3 , falling in the backfill sand's typical value for use in road construction works (Jamsawang et al. 2015, 2018). Comparisons of the grain size distribution curves of the raw materials in Fig. 2, obtained from sieve and laser analyses, indicate that the mean particle size values of the sediment, cement, and fly ash were 0.85, 0.014, and 0.019 mm, respectively. Thus, the sediment's mean particle size was 50 times greater than that of cement and fly ash. The fly ash acts as both a pozzolan and a filter in the sediment pore space.

Table 2 shows the chemical compounds of raw sediment, cement, and fly ash derived from XRF analyses. The fly ash is characterized as class C because the sum of its SiO_2 , Al_2O_3 , and Fe_2O_3 fractions is 69.14% (ranging from 50 to 70%), based on ASTM C 618. The fly ash can also contribute cementitious and pozzolanic properties since it is comprised of both 17.85% CaO and 37.34% SiO_2 contents. As a result, fly ash alone can be an admixture for enhancing sediment properties. Cement contains an excellent CaO content of 66.35%, which is more significant than the CaO content in fly ash. Therefore, cement alone is a primary source of cementitious properties and can effectively stabilize sediments in short-term conditions. In this study, fly ash-blended cement is more useful than sole cement due to the high SiO_2 content in the fly ash, which actively reacts with the CaO in cement to deliver long-term strength via the pozzolanic reaction.

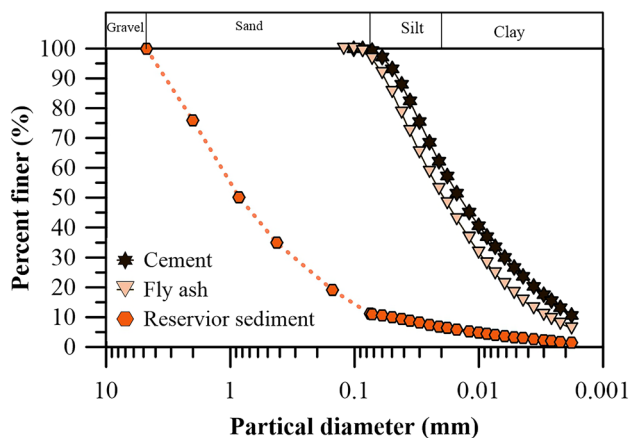


Fig. 3 Grain size distribution curves of the raw materials used in this study

Table 1 Geotechnical properties of raw reservoir sediment

Property	Value
Natural moisture content (%)	75
Liquid limit (%)	47
Plastic limit (%)	39
Plasticity index (%)	8
Specific gravity	2.75
Maximum dry unit weight (kN/m^3)	16.5
Optimum moisture content (%)	18.5
Soil classification (USCS)	SW-SM

Preparing and molding samples

The raw sediments, which have a high natural moisture content, were air-dried for 24 h, shaken through a sieve with a 4.75-mm opening size to remove the gravel particles, and later oven-dried for 24 h to obtain a zero initial moisture content before molding. All mechanical tests were performed utilizing cement alone, fly ash alone, and fly ash-blended cement. Cement contents of 1.5, 2.5, 5, and 7.5% (by dry sediment weight) and fly ash contents of 5, 10, 15, and 20% (by dry sediment weight) were employed to mix with the prepared sediments. Notably, the fly ash and cement contents used in this study were selected based on previous similar studies and several prior attempts by the authors during preliminary inquiry (Yoobanpot et al., 2020a, b; Jamsawang et al., 2021). The mixture's water content attains the optimum moisture content of 18.5%, derived from modified Proctor compaction tests. All mixture proportions were tested in triplicate for each testing condition, as listed in Table 3. The cylindrical molding samples for the unconfined compression (UC), indirect tensile (IT), wetting and drying cycles (WDC), resilient modulus (M_r), and free-free resonance (FFR) tests had diameters of 50 mm and heights of 100 mm, whereas those for the CBR tests had diameters of 152 mm and heights

Table 2 Chemical composition of the reservoir sediment, cement, and class C fly ash

Compound	Reservoir sediment (%)	Cement (%)	Class C fly ash (%)
Silicon dioxide (SiO_2)	65.60	18.43	37.34
Alumina oxide (Al_2O_3)	17.5	4.95	18.63
Ferric oxide (Fe_2O_3)	9.81	3.29	13.17
Calcium oxide (CaO)	0.75	66.35	17.85
Magnesium oxide (MgO)	1.43	0.86	3.92
Sulfur trioxide (SO_3)	0.20	3.18	3.51
Potassium oxide (K_2O)	2.56	1.22	2.52
$\text{Na}_2\text{O} + \text{TiO}_2 + \text{other}$	1.34	0.15	2.42
Loss on ignition (% by mass)	0.81	1.57	0.64

Table 3 Mixture proportion

Designation	Fly ash content (%)	Cement content (%)	Dry sediment content (%)
Unsolidified	0	0	100
Sole fly ash			
F5	5	0	95
F10	10	0	90
F15	15	0	85
F20	20	0	80
Sole cement			
C1.5	0	1.5	98.5
C2.5	0	2.5	97.5
C3.5	0	3.5	96.5
C5	0	5.0	95.0
Fly ash blend cement			
F5-C1.5	5	1.5	93.5
F5-C2.5	5	2.5	92.5
F5-C3.5	5	3.5	91.5
F5-C5	5	5.0	90.0
F10-C1.5	10	1.5	88.5
F10-C2.5	10	2.5	87.5
F10-C3.5	10	3.5	86.5
F10-C5	10	5.0	85.0
F15-C1.5	15	1.5	83.5
F15-C2.5	15	2.5	82.5
F15-C3.5	15	3.5	81.5
F15-C5	15	5.0	80.0
F20-C1.5	20	1.5	78.5
F20-C2.5	20	2.5	77.5
F20-C3.5	20	3.5	76.5
F20-C5	20	5.0	75.0

All mixture proportions were tested on 3 replicated samples for each testing condition

of 116 mm. All dry mixtures were prepared by hand mixing of dry sediment, cement, and fly ash for 5 min, and water was later gradually added to the dry mixtures by spraying. The dry mixes and water were hand mixed again for 5 min until uniform and homogeneous mixtures were visually observed.

Each sample for the UC, IT, WDC, M_r , and FFR tests was molded by containing each prepared mixture in a cylindrical split stainless mold lubricated inside with grease. The sample was subsequently statically compressed in three layers using a compression machine until each layer achieved the maximum dry unit weight of 16.5 kN/m^3 , derived from modified Proctor compaction tests. After completing the sample molding process, the sample was carefully removed by splitting the mold into two pieces to minimize sample damage. Once removed, each specimen was instantly wrapped with plastic wrap to prevent sample moisture loss. The covered sample was then cured for 7, 14, 28, 60, and 120 days inside

a storage cabinet under a controlled room temperature of $40 \pm 2 \text{ }^\circ\text{C}$ to emulate Thailand's weather.

When the assigned curing time of the specimen for each test was achieved, the test was then immediately performed. The acceptance criterion was designated that the individual test values of three samples, molded with the same characteristics, must deviate from the mean test value by less than 10% to avoid the error caused by the discreteness of the sample. For all tests in this study, an average value of the test results based on three specimens was reported.

Experiments

This section describes the UC, IT, WDC, M_r , and FFR experimental details and procedures. After the assigned curing time of the sample was achieved, the experiments were immediately performed. The test results' average value based on three replicates was reported for all experiments in this study. All the tests were performed using an automatic loading machine with a capacity of 50 kN, brand "Controls with V1072 series multispeed digital version." The machine consisted of a stand-alone automatic digital load frame with a 50-kN capacity. Electric motors with closed-loop speed control were used to control the deformation rate during each test and provided a fully variable test speed of 0.2 to 51 mm/min. The machine can be equipped with analog or digital load/displacement measurement systems and specific accessories to suit either the field or central laboratory requirements. Electric load cells of brand "Kyowa" and linear variable differential transducers (LVDTs) by "Kyowa" were utilized to measure the applied loads and deformations of the specimens. The electric data logger system, brand "Kyowa" model UCAM-550A, was used because it is a fast data logger that repeatedly measures a maximum of 1000 channels at an interval of 0.02 s and supports load and displacement transducers. Measuring channels are for 1 unit, a maximum of 50 channels, and with 20 cascaded units, a maximum of 1000 channels, and these are suited for small-scale to large-scale measurements. Therefore, the electric data logger used in this study can provide sufficient measurement data to create precise stress–deformation curves for assessing the reliability of the mechanical performance of the tested specimen and for the interpretation of the accuracy of the results.

Unconfined compression tests

The UC tests were performed based on ASTM D 2166 (2016a) to generate unconfined compressive stress–axial strain curves for determining the q_u and the secant modulus (E_{50}) values of the specimens. A 50-kN-capacity load cell and a 50-mm-capacity LVDT were used. A vertical

displacement rate of 1 mm/min was applied to the test sample until 15% axial strain was attained. The q_u is defined as the maximum compressive stress when the stress–strain curve exhibits apparent peak stress. Otherwise, q_u is examined as the compressive stress at 15% axial strain. The E_{50} is estimated from the stress–strain curve slope and is defined as the secant modulus at 50% q_u , according to a safety factor of 2.

Indirect tensile tests

According to ASTM D 3967 (2016b), IT tests were performed to determine the q_t value of the solidified samples. Each specimen was placed in direct contact with two steel-bearing strips. A 20-kN-capacity load cell with a vertical displacement rate of 1.00 mm/min was utilized to obtain the accurate failure load. The load was applied to the specimen from the top to produce a vertical crack along with the sample diameter induced by splitting tension. q_t was defined as follows: $q_t = 2P/\pi dl$, where q_t is the indirect tensile strength, P is the compressive load at failure, d is the sample diameter, and l is the sample length.

Resilient modulus tests

The M_r tests were performed under the AASHTO T307 (2012) standard test method to determine the M_r of both unsolidified and solidified specimens. The M_r test apparatus was comprised of two 20-mm-capacity LVDTs placed symmetrically on the sample's top to detect the vertical displacements. A 10-kN-capacity load cell mounted on the loading piston with a vertical displacement rate of 1.00 mm/min was utilized to create the deviatoric stress–axial strain curve. The test was finished when a total vertical permanent strain of 5% was obtained. A pressurized air chamber was used to generate confining pressures for accommodating the specimen throughout testing. Axial cyclic stress with a constant magnitude of 0.1 s, followed by a 0.9-s rest period, was applied to the test sample. A loading cycle of 1 s is composed of a stress and rest period, representing a 1-Hz frequency. Each specimen was subjected to preconditioning, including a 103.4-kPa confining pressure, 93.1-kPa deviatoric stress, and 10.3-kPa contact stress with 500-cycle stress repetitions. The specimen was subsequently subjected to 15 sequences of applied stress conditions, consisting of five distinct confining pressures and three different deviatoric stresses for each confining pressure with 100-cycle stress repetitions, as listed in Table 4. The M_r value for each sequence was determined by considering the average of the previous five records. In contrast, the M_r value reported for the designated specimen was based on the average value derived from 15 sequences (Mamatha and Dinesh 2017).

Table 4 Resilient modulus testing sequences

Test sequence	Confining pressure (kPa)	Deviator stress (kPa)	Contact stress (kPa)
0 (preconditioning)	103.4	93.1	10.3
1	20.7	18.6	2.1
2	20.7	37.3	4.1
3	20.7	55.9	6.2
4	34.5	37.0	3.5
5	34.5	62.0	6.9
6	34.5	93.1	10.3
7	68.9	62.0	6.9
8	68.9	124.1	13.8
9	68.9	186.1	20.7
10	103.4	62.0	6.9
11	103.4	93.1	10.3
12	103.4	186.1	20.7
13	137.9	93.1	10.3
14	137.9	124.1	13.8
15	137.9	248.2	27.6

California bearing ratio tests

The CBR tests were operated per ASTM D1883 (2016c). Each mix was dynamically compacted in a standard compaction steel mold, following a modified Proctor compaction test. The compacted sample in the mold with a 45-kN surcharge was soaked for 96 h to emulate the road material characteristics when subjected to rainfall or flooding conditions. After the specimen was completely soaked, the penetration piston load was applied to the soaked sample with a 1.27 mm/min penetration rate using a 20-mm-capacity LVDT to create a penetration stress–penetration curve. The CBR is defined as the test stress at either a 2.54 mm or 5.08 mm penetration divided by the corresponding standard stress of either 6900 or 10,300 kPa multiplied by 100%, respectively. The CBR is usually reported based on the value at a 2.54-mm penetration. If the CBR at 5.08 mm penetration is larger than that at 2.54-mm penetration, retesting will be needed. However, the CBR at 5.08-mm penetration will be reported if the retest shows similar results.

Wetting and drying cycle tests

The ASTM D559 (2015) standard test method was adapted for the specimen preparation for WDC tests. In a cycle of the wetting and drying process, each solidified sample was preliminarily soaked at room temperature for 5 h, then oven-dried at 71 °C for 42 h, and subsequently cooled to room temperature for 3 h. A total number of three samples were required for each mix to complete the tests. The first, second,

and third samples were subjected to 1, 3, and 6 WDCs. After each assigned cycle was attained, the prepared specimen was instantly soaked in water at 25 °C for 1 h. The UC test was subsequently conducted on the soaked sample following “Unconfined compression tests” to determine the residual q_u under 1, 3, and 6 WDCs, designated as $q_{u(WDC)}$.

Free–free resonance tests

The FFR tests were performed based on an adaptation of the ASTM C215 (2019) standard test method for the determination of the V_p and V_s of both unsolidified and solidified samples. Before the destructive UC and IT tests were performed, the same specimen was employed for the nondestructive FFR tests to ensure that the destructive and nondestructive test results were based on similar specimen conditions. Thus, the relationships among them were reliable. The specimen was freely mounted on a rigid frame in the horizontal direction and suspended with a tendon to approach free boundary conditions. An accelerometer was set in contact with one end of the sample, while another end was knocked with a light hammer. The following relationships can be used to calculate V_p and V_s : $V_p = 2lf_p$ and $V_s = 2lf_s$, where l is the specimen length, f_p is the resonant frequency induced by a compressive wave, and f_s is the resonant frequency caused by a shear compressive wave. The wavelength is two times the sample length when the sample with a length-diameter ratio of 2 is subjected to a free vibration with both ends free (Ryden et al. 2006). The theory of one-dimensional wave propagation in an elastic rod was adapted to estimate the dynamic Young's modulus (E_0) and shear modulus (G_0) of the test specimen. E_0 and G_0 can be evaluated based on the sample's measured V_p and V_s with the sample's density (ρ) using $E_0 = \rho V_p^2$ and $G_0 = \rho V_s^2$ (Nazarian et al. 1999). The dynamic Poisson's ratio (ν_0) can also be derived $\nu_0 = (E_0/2G_0) - 1$ based on the assumption of a linear-elastic, homogeneous, and isotropic material.

Microstructural analyses

X-ray diffraction analyses

XRD analyses were performed on both unsolidified and solidified samples. The small samples for XRD analyses were extracted from the test specimens' failure surfaces after the UC tests were accomplished. The retrieved piece was then placed in a desiccator on silica gel to be air-dried for 24 h. The dried sample was then ground with a medicine grinder to prepare a powder material, and the powder material was then sieved through a 0.075-mm sieve (no. 200 sieve) until 20 g of powder finer than 0.075 mm was obtained. XRD analysis was performed on the fine powder

by a Siemens D-500 XRD instrument with Stirling equipment and Cu K α radiation at 40 kV and 30 mA. Intensity data were recorded every 0.02° from 2 to 80°.

Thermogravimetric analyzer analyses

TGA analysis was performed on the solidified samples utilizing the STA 449F3–Jupiter equipment. The specimen preparation was similar to the XRD analyses. The 100-mg powdered sample was placed on a balance located in the furnace. The heating process was subsequently applied over the temperature range from 25 to 750 °C under a 10 °C/min heating rate in a flowing nitrogen environment.

Scanning electron microscopy–energy-dispersive X-ray spectrometry analyses

SEM–EDX analyses were conducted on both unsolidified and solidified samples to investigate the change in elemental composition/distribution induced by hydration and pozzolanic reactions. A small rectangular piece of the sample with approximate dimensions of 5 mm \times 5 mm \times 2 mm was collected from the same specimens as the XRD analyses. The acquired sample was placed in a desiccator on silica gel to be air-dried for 24 h and was then coated with platinum over 30 s at a current of 50 mA. SEM micrographs with 3500 times magnification were derived with Do SEM JSM-5410 LV equipment. EDX analysis was then conducted on the corresponding SEM micrograph regions with a Do SEM Link ISIS300 instrument.

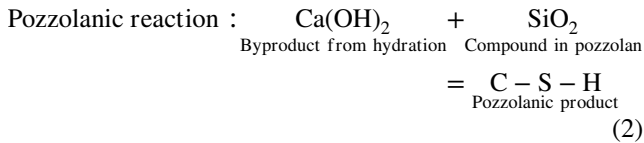
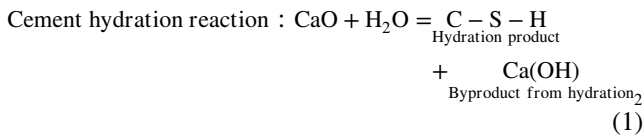
Test results

Destructive properties

Unconfined compressive strength

A strength increase in sediments solidified with fly ash and cement is expressed through the primary cement hydration reaction (Eq. 1) and secondary pozzolanic reaction (Eq. 2). The cement hydration reaction develops early after fly ash–cement blend and sediment are mixed with the optimum water content, produced by the CaO segregation from cement and fly ash particles. SiO₂ in the cement is disintegrated by high CaO concentrations. The cement hydration products subsequently create calcium silicate hydrate (C–S–H) gel and calcium hydroxide (Ca(OH)₂). The C–S–H gel is a cementitious substance that gives adhesive properties to the sediment particles, while Ca(OH)₂ is a byproduct of the cement hydration process. The pozzolanic reaction later develops since the SiO₂ in fly ash continuously adsorbs the Ca(OH)₂ obtained from the cement hydration reaction. The

pozzolanic reaction products (additional C-S-H gels) are consequently generated.



The strength increase characteristics are highly dependent on the C-S-H product amounts derived from either the cement hydration reaction or pozzolanic reaction. The C-S-H products induced by the cement hydration reaction provide a short-term strength increase. In contrast, the C-S-H products from the pozzolanic reaction give a long-term strength increase (Horpibulsuk et al. 2009; Kang et al. 2014; Shon et al. 2010; Tastan et al. 2011; Wang et al. 2013). The C-S-H gels bind the reservoir sediment particles together, providing strong cohesiveness to the sediment matrix. This phenomenon results in a strength increase with increasing C-S-H products.

In summary, fly ash-cement blend was most effective in solidifying the sediment, followed by sole cement and sole fly ash. Based on Eqs. 1 and 2, the fly ash-blended cement provided the most extensive C-S-H contents because the C-S-H contents were derived from a combination of C-S-H contents produced from both cement hydration and pozzolanic reactions. The 10% fly ash revealed the best q_u values for all mixes, including F10-C1.5, F10-C2.5, F10-C3.5, and F10-C5, because the 10% fly ash gave the most suitable SiO_2 and CaOH_2 portions obtained from the fly ash and cement hydration reaction, respectively. Therefore, the 10% fly ash caused the highest pozzolanic reaction level, creating the most extensive C-S-H products. However, fly ash over 10% can block cement particles, preventing water and cement chemical reactions. This occurrence reduces the C-S-H products, and q_u subsequently decreases (Horpibulsuk et al. 2011a, b). The use of sole cement yielded a smaller q_u than the fly ash-cement blend because most C-S-H products were derived from the cement hydration reaction only due to the absence of SiO_2 in FA. The sole fly ash gave the smallest q_u because of the lack of CaO from cement to produce the C-S-H products in the cement hydration reaction, resulting in the lowest C-S-H amounts.

Figure 4a shows the effect of fly ash and cement contents on the q_u of solidified samples for various curing periods of 7 to 120 days. The q_u values for all mixes regularly increased with the curing period. Notably, the q_u values of the specimens solidified with sole cement grew with the cement contents. In contrast, sole fly ash and fly ash-cement blend

solidifications were characterized as two principal regions, including active and degradable zones. The strengths and moduli increased clearly with increases in the fly ash content in the active zone and attained maximum strength and modulus values at 10% fly ash. However, the strengths and moduli continuously decreased as the fly ash content exceeded 10% in the degradable region. Although the strengths and moduli increased compared to the unsolidified sample, in which the rate of increase was relatively low. Thus, the solidification in the degradable zone was uneconomical compared to that in the active region. For the short-term q_u of the 28-day curing time, the q_u values of the samples solidified with sole 10% fly ash (F10), sole 5% cement (C5), and 10% fly ash-cement blend (F10-C5) were 0.8, 3.2, and 3.6 MPa, respectively. As the curing period increased to 120 days, the long-term q_u increased to 3.1, 4.4, and 6.8 MPa for F10, C5, and F10-C5, respectively.

Indirect tensile strength

Figure 4b shows that the q_t and q_u values of the solidified specimens exhibited similar strength evolution trends. The q_t of the unsolidified sample was 0.09 MPa. In contrast, the 28-day q_t values were found to be 0.25, 0.46, and 0.57 MPa, and the 120-day q_t values were equal to 0.50, 0.74, and 1.09 MPa for F10, C5, and F10-C5, respectively. Figure 5a presents the relationship between the q_t and q_u of solidified sediments for q_t variations between 0.12 and 1.09 MPa and q_u between 0.82 and 6.84 MPa. The q_t value was 1.3 to 12.1 times greater than that of the unsolidified sample. The q_t - q_u correlation for the solidified reservoir sediments was expressed as $q_t = 0.16q_u$, which was within the range of $q_t = 0.1-0.2q_u$ for solidified soils with cementitious materials, as reported in previous studies (Baldovino et al. 2018; Consoli et al. 2014; Koliass et al. 2005).

California bearing ratio

The CBR results in Fig. 4c show similar trends to the q_u results of the solidified sediments. The CBR value of the unsolidified sample was 6%. In contrast, the solidified sediments with sole fly ash, sole cement, and fly ash-cement blend had variations in CBR values of 16–50%, 30–106%, and 32–136%, respectively. The empirical relationship between the CBR and the q_u value derived from the current study is shown in Fig. 5a. The correlation varies from $\text{CBR}(\%) = 10-30q_u(\text{MPa})$, and the best fit is $\text{CBR}(\%) = 20q_u(\text{MPa})$, which falls in the range of generally treated soils as proposed by Agapitus (2014); Jiang et al. (2016); Voottipruex and Jamsawang (2014); Yoobanpot et al. (2018).

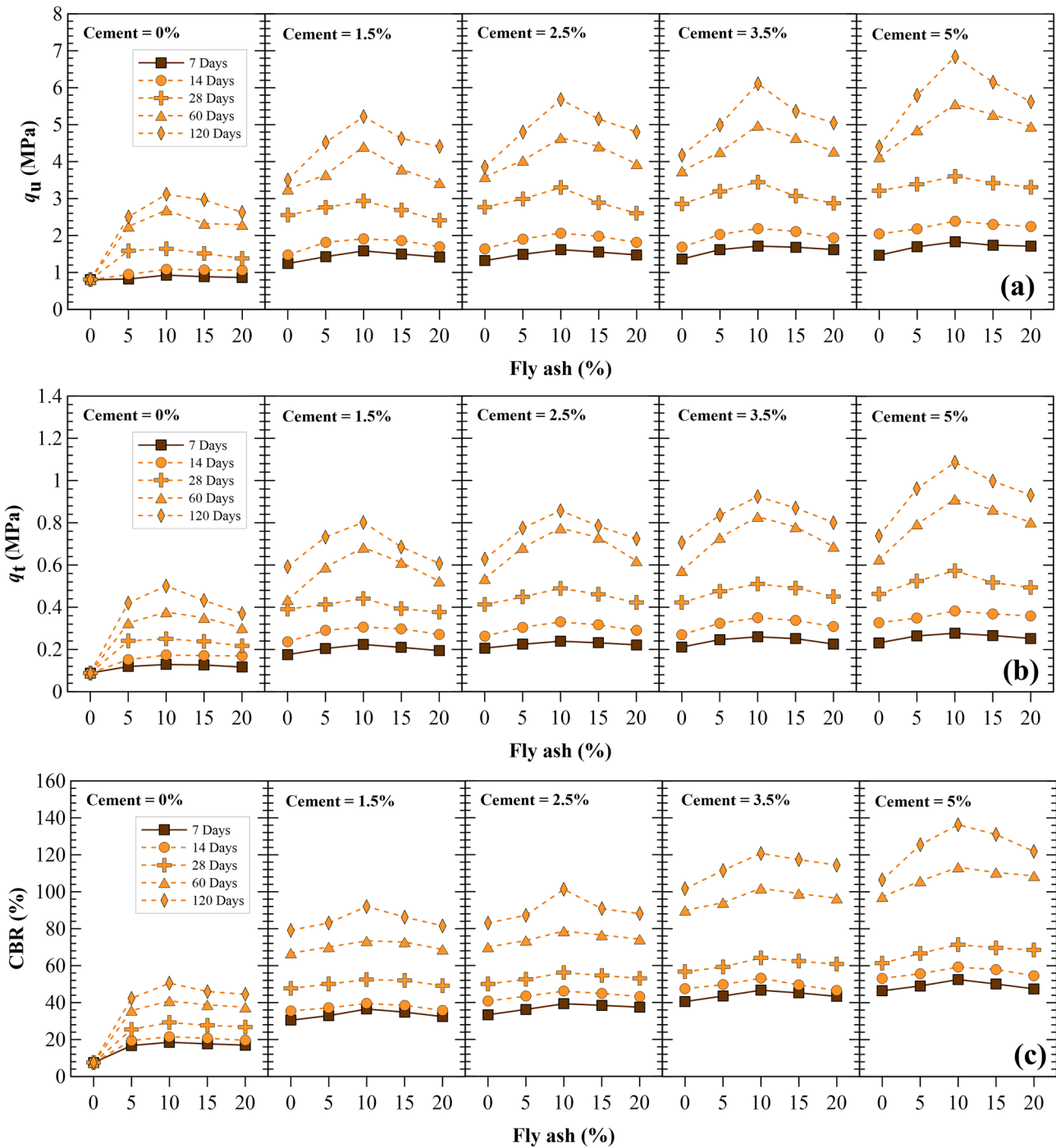


Fig. 4 Destructive properties versus curing times

Strain at failure

Figure 4d shows that the strain at failure (ϵ_f) values of solidified samples decreased as the curing time increased, indicating that the degree of the specimens' brittleness

increased with increasing time. Most values of ϵ_f were distributed in the range of 2 to 3.2%. The specimens' brittleness significantly depends on their q_u magnitudes and exhibits inverse variation to the q_u values. Thus, an increase in q_u induced brittleness in solidified samples,

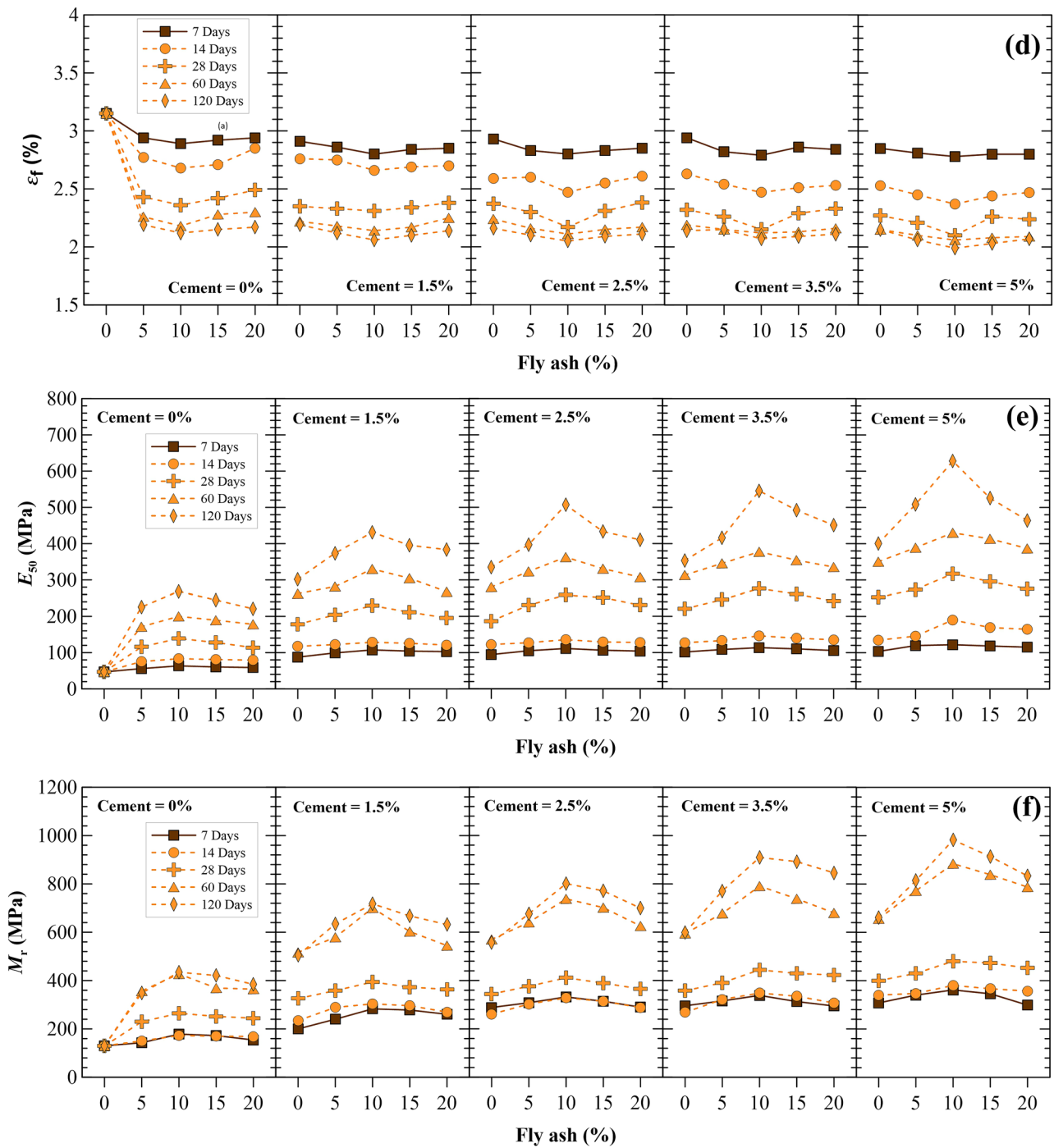


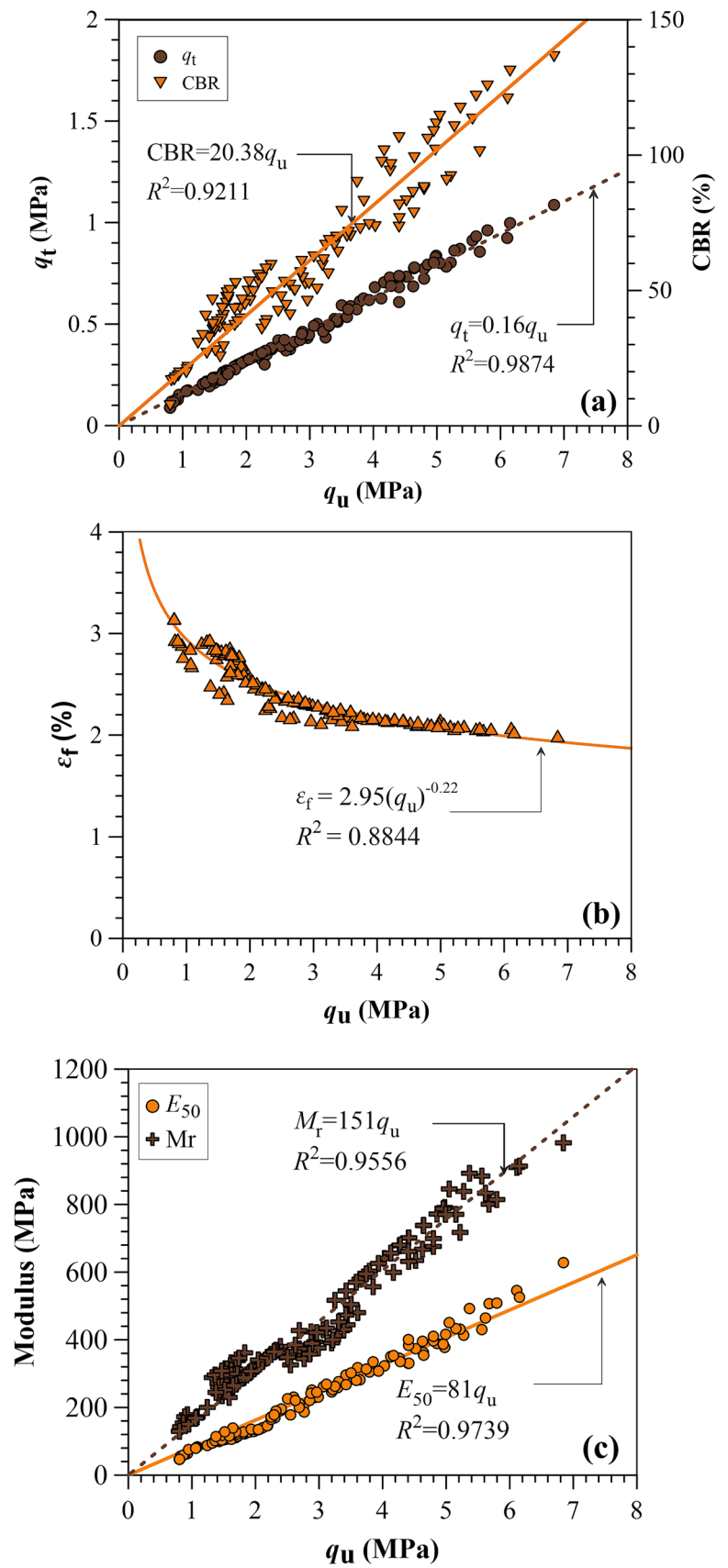
Fig. 4 (continued)

decreasing ϵ_f . The correlation between the ϵ_f and q_u values found in the current is presented in Fig. 5b. The ϵ_f - q_u correlation of the solidified sediment obtained from this study is well represented by a power function, expressed by $\epsilon_f = 2.95q_u^{-0.22}$. This relationship corresponds to that reported by Al-Mukhtar et al. (2010b) for cement-stabilized zinc-contaminated clays.

Secant elastic modulus

The evolution of the E_{50} of solidified sediments in Fig. 4e shows that the variations in E_{50} values were consistent with the q_u values for the designed samples. The variations in E_{50} values were 56–628 MPa for q_u values of 0.82–6.84 MPa. The E_{50} - q_u linear correlation in the current study is

Fig. 5 Correlation between destructive properties and q_u



presented in Fig. 5c, represented by $E_{50} = 81q_u$. Solidified marine clay with cement-blended metakaolin showed a brittle response with a relation of $E_{50} = 160q_u$ (Tongwei et al. 2014), overestimating the linear correlation derived from the current study by a factor of two. In contrast, marine sediment solidified with cement-blended lime and fly ash exhibited semiductile behavior with a correlation of $E_{50} = 60q_u$ (Wang et al. 2013), underestimating the current study result by a factor of 1.4. However, a similar correlation was reported for soft clay solidified with cement replaced with bagasse ash (Jamsawang et al. 2017a). The greater-strength sample exhibits a greater E_{50} level due to its high degree of brittleness. Typically, E_{50} depends on various factors, including the soil property, stress history, soil fabric, interparticle contact stiffness, effective stress particle roughness, and particle angularity (Verástegui–Flores et al. 2015).

Resilience modulus

Figure 4f reports the M_r values after 15 cycles, revealing the same characteristics as those of the E_{50} values. The M_r value of the unsolidified sample was 130 MPa. After solidification with fly ash alone, cement alone, and fly ash–cement blend, the M_r values increased to 140–430, 200–660, and 240–980 MPa, respectively. The M_r – q_u correlation of the current study in Fig. 5c shows that M_r increased proportionally with q_u , similar to the E_{50} – q_u correlation. A linear correlation can be reasonably used for modeling M_r – q_u relationships (Austroads 2017), which is expressed as $M_r = 151q_u$. The linear regressions found by other researchers were $M_r = 70$ – $270q_u$ for fly ash-treated organic soils, quick lime-stabilized silty soils, and clayey soils solidified with cement, lime, and fly ash (Ardah et al. 2017; Arora and Aydilek 2005; Tastan et al. 2011), which are the lower and upper limits of the linear correlation derived from the current study.

Nondestructive properties

Compression wave velocity and shear wave velocity

Figure 6a and b present the V_p and V_s assessed from the FFR tests versus curing periods, respectively. In general, V_p and V_s increased with the curing time due to the strength development over time of the solidified sediments (Yesiller et al. 2001). The values of V_p and V_s were between 375–1330 m/s and between 195–730 m/s, respectively, for the q_u values of 0.82–6.84 MPa. The V_p and V_s propagations occur along the fastest pathway in the solidified samples. Therefore, they depend on the static stiffnesses, which are affected by similar factors, including particle bonding, porosity, and microstructure (Larsson 2005). The variations in V_p and V_s of the solidified samples are possibly

related to the sediment homogeneity, uniformity of admixture distribution, and the existence of specific unmixed sediment inclusions (Guimond–Barrett et al. 2013). The V_p – q_u and V_s – q_u relationships from the present research in Fig. 7a illustrate the power–law functions as follows: $q_u(\text{MPa}) = 0.00007V_p^{1.92}(\text{m/s})$ and $q_u(\text{MPa}) = 0.00002V_s^{1.92}(\text{m/s})$, respectively.

Dynamic Young's modulus and shear modulus

Figure 6c and d illustrate the influences of the cement and fly ash contents and the curing periods on the E_0 and G_0 values of the solidified specimens, respectively. The E_0 and G_0 values varied from 32 to 227 MPa and 9 to 68 MPa, respectively. The unsolidified sediment had E_0 and G_0 values of 29 and 8 MPa, respectively. For all mixes, E_0 and G_0 increased as the particular cement and fly ash contents and curing period increased, and E_0 and G_0 achieved maximum values at a fly ash content of 10%. E_0 and G_0 gradually decreased when the fly ash content exceeded 10%, which exhibited similar characteristics as those of the E_{50} values.

Consequently, F10-C5 provided maximum E_0 and G_0 values of 97 and 227 MPa and 28 and 68 MPa for curing times of 7 and 120 days, respectively. As the curing periods increased, the bonding development between the sediment particles was created due to the increasing hydration and pozzolanic reactions. This phenomenon increased the number of contact points between the sediment particles and reduced the number of voids in a solidified sample (Aldoood et al. 2014; Al-Mukhtar et al. 2010a, b), which affected V_p and E_0 . Similarly, V_s and G_0 also increased since the solidified samples' skeletal stiffnesses formed after a curing time of 28 days (Meei–Hoan and Chee–Ming 2014). E_0 and G_0 are plotted versus q_u in Fig. 7b. In the range of the unconfined compressive strength tests, E_0 and G_0 increased linearly with q_u . The ratios of E_0 and G_0 to q_u for the present study were found to be 33 and 10, respectively.

Dynamic Poisson's ratio

Figure 6e shows the relationship between ν_0 and q_u for all mixes at curing periods of 7, 14, 28, 60, and 120 days. The values of ν_0 for the solidified samples were between 0.255 and 0.346, corresponding to an average of 0.297. The unsolidified sediment had a ν_0 of 0.312, whereas the unsolidified specimens had ν_0 values of 0.255 to 0.346, corresponding to an average value of 0.297. The typical ν_0 values for sandy clay, silt, and sand were found to be 0.25, 0.325, and 0.375, respectively, as Bowles (1997) reported. Thus, the ν_0 value of unsolidified sediment was close to that of silt. However, the ν_0 values decreased in the sandy clay and silt ranges after solidifying with the fly ash–cement blend. No clear correlation between ν_0 and q_u was observed in this study,

Fig. 6 Nondestructive properties versus curing times

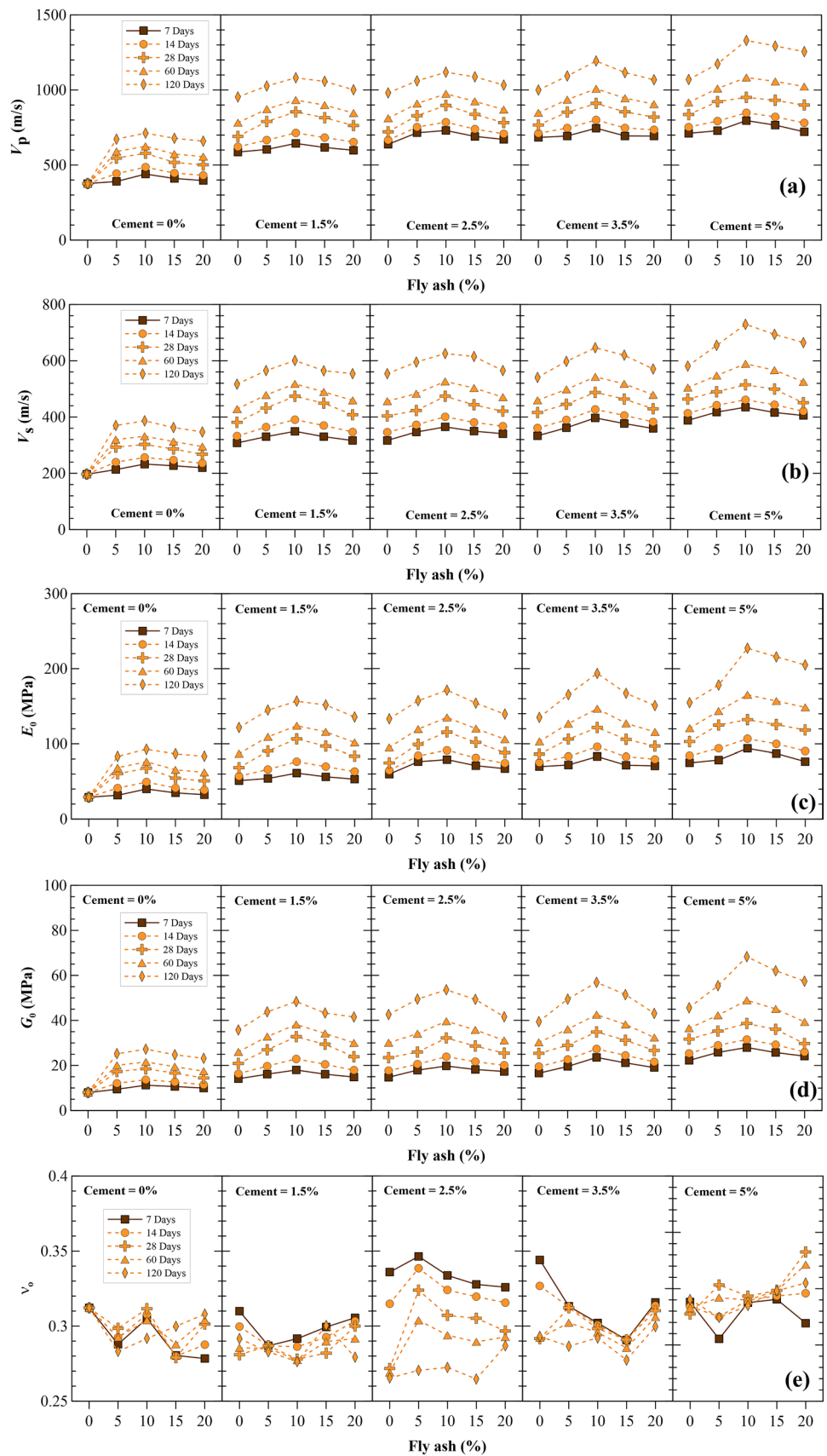
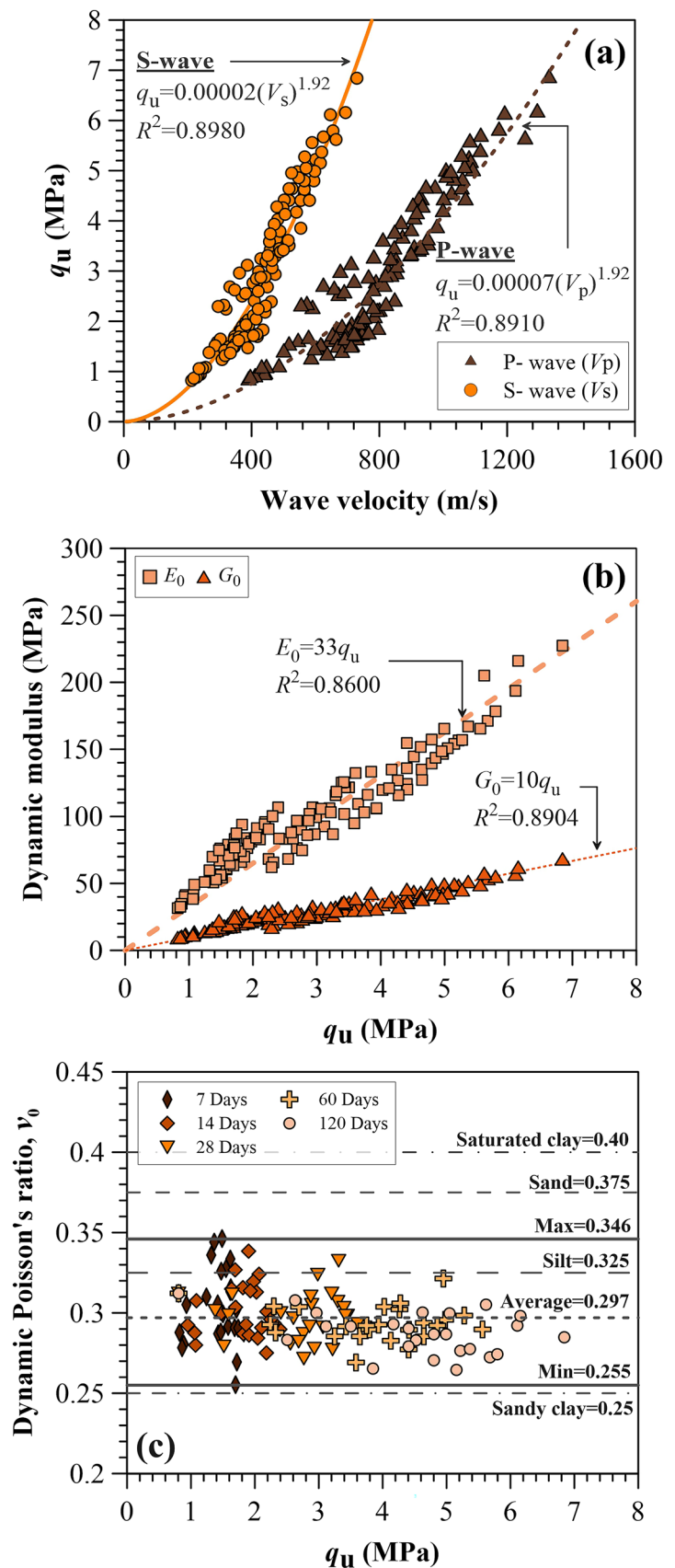


Fig. 7 Correlation between non-destructive properties and q_u



unlike the E_0-q_u and G_0-q_u correlations. Thus, ν_0 depends on the property of the base sediment rather than that of the solidified sediment.

Wetting and drying cycles

Figure 8a illustrates the $q_{u(WDC)}$ of all solidified samples subjected to 1, 3, and 6 wet–dry cycles for curing periods of 7, 28, and 60 days, which is compared to the q_u of corresponding solidified specimens without wet–dry processes (0 wet–dry cycles, derived from Fig. 4a). Regarding the samples with a 28-day curing time, the $q_{u(WDC)}$ values of F10, C5, and F10-C5 subjected to 1 wet–dry cycle were 1.5, 1.9, and 2.2 MPa, respectively. As the sample curing time increased to 60 days, $q_{u(WDC)}$ increased to 2.3, 2.5, and 3.6 MPa for F10, C5, and F10-C5, respectively. This phenomenon indicates that $q_{u(WDC)}$ and q_u had similar strength development characteristics. The $q_{u(WDC)}$ for all samples decreased significantly with the number of wet–dry cycles (C_{WD}). For example, the $q_{u(WDC)}$ values of F10, C5, and F10-C5 subjected to 6 wet–dry cycles were 0.29, 0.36, and 0.49 MPa (28-day curing time), and 0.58, 0.59, and 1.07 MPa (60-day curing time), respectively. Therefore, the $q_{u(WDC)}$ values significantly depend on the q_u values. The

wetting causes clay particle swelling due to the expansion of the diffuse double layer (Kampala and Horpibulsuk 2013; Kampala et al. 2014; Tang et al. 2011). In contrast, the drying process reduces the pore volumes due to the water loss in voids between the solid particles, resulting in shrinkage and surface cracks on the solidified samples (Kampala and Horpibulsuk 2013; Kampala et al. 2014; Tang et al. 2011). Thus, the expansion, shrinkage, and surface cracks caused by the wet–dry cycles reduced the strength of the solidified sediment.

The number of cracks increased with an increasing C_{WD} , as shown in Fig. 8b, resulting in a decrease in strength with growing wet–dry processes. The correlation between the normalized strength, $q_{u(WDC)}/q_u$, and C_{WD} is presented in Fig. 8c and given by the following equation: $q_{u(WDC)}/q_u = 0.694 - 0.1C_{WD}$. The C_{WD} value may be different, depending on the soil type or road materials. For example, the use of 1 to 12 C_{WD} is suitable for cement-treated soils used as a base course (PCA 1992), or the use of 1 to 4 C_{WD} is recommended for silty and clayey soils (Tripathy et al. 2009). COE (2004) suggests that $q_{u(WDC)}$ values must be more than 1,723 and 2,068 kPa at curing periods of 7 and 28 days, respectively. Thus, the use of 6 C_{WD} samples was sufficient for solidified sediments in this study because the

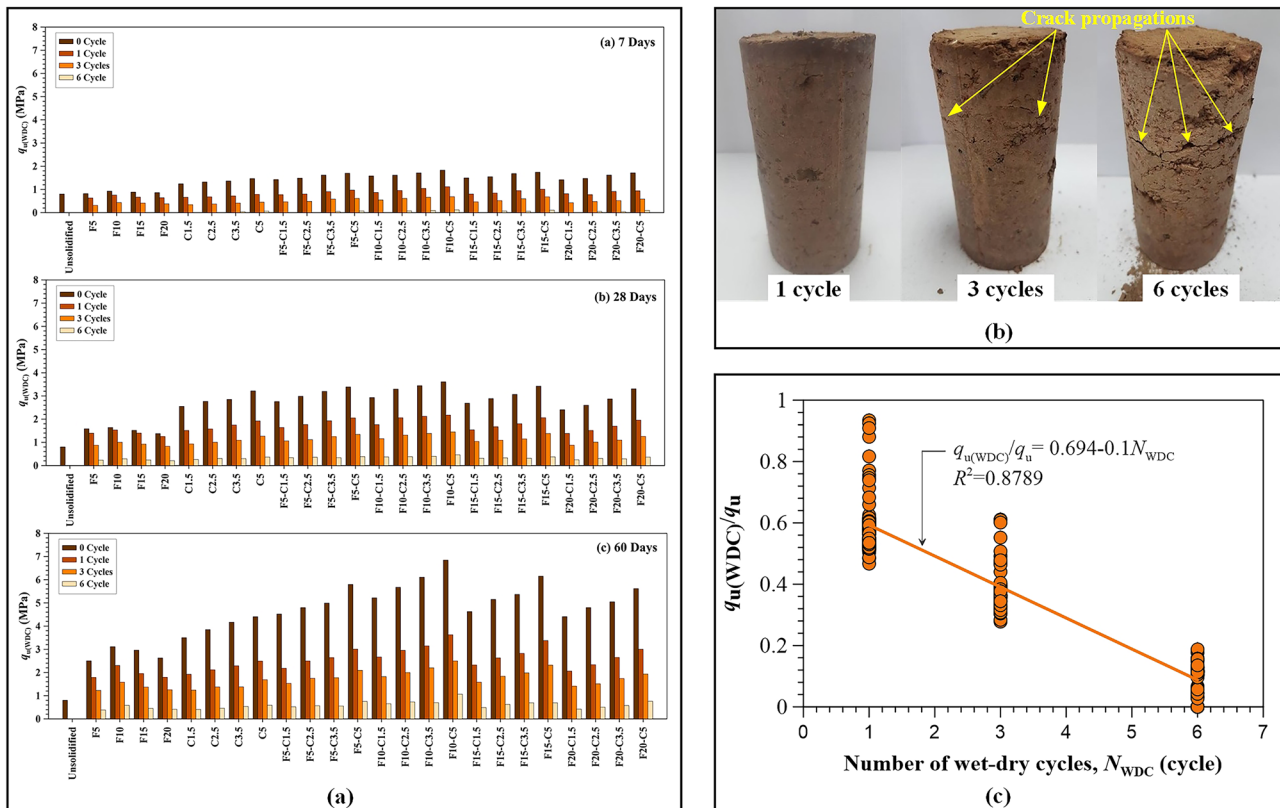


Fig. 8 a Effect of the fly ash-blended cement on the $q_{u(WDC)}$ values, b crack propagation of the samples subjected to 1, 3, and 6 WDC, and c relationship between the normalized strength and N_{WDC}

$q_{u(WDC)}$ values of the samples subjected to 6 C_{WD} samples were lower than the values specified by COE (2004).

Normalized destructive and nondestructive characteristic development with time

Based on the results in “Destructive properties” and “Non-destructive properties” the destructive and nondestructive properties of reservoir sediments solidified with fly ash alone, cement alone, and fly ash–cement blend characteristics developed with curing time caused by the results of hydration and pozzolanic reactions. The destructive and non-destructive strength and modulus properties of the solidified sediments at 28 days, $strength_{(28D)}$ and $modulus_{(28D)}$, including $q_{u(28D)}$, $q_{t(28D)}$, $\epsilon_{f(28D)}$, $CBR_{(28D)}$, $E_{50(28D)}$, $M_{r(28D)}$, $E_{0(28D)}$, and $G_{0(28D)}$, were employed to normalize the development of the properties of the solidified sediments after a curing period of D days, $strength_{(D)}$ and $modulus_{(D)}$, including $q_{u(D)}$, $q_{t(D)}$, $\epsilon_{f(D)}$, $CBR_{(D)}$, $E_{50(D)}$, $M_{r(D)}$, $E_{0(D)}$, and $G_{0(D)}$. The normalized development of such properties for the solidified sediments is illustrated on a natural logarithmic scale by linear correlations (Horpibulsuk et al. 2009, 2011a, b, 2012; Yoobanpot et al. 2017, 2018), as given in Fig. 9a–c.

Microscopic analysis results

X-ray diffraction

Figure 10a and b show the XRD patterns of the unsolidified sample (F0-C0), solidified specimens with cement only (C5), and fly ash–cement blend (F10-C5 and F20-C5) after short-term curing for 28 days and long-term curing for 120 days, respectively. The C–S–H peaks of solidified samples at 28 and 120 days of curing. The increases in strength and moduli due to increasing C–S–H product amounts, derived from cement hydration reaction and pozzolanic reactions, as discussed in “Destructive properties” are verified by observing the C–S–H peak intensities at the reference reflections (Jamsawang et al. 2017b; Mutaz and Dafalla 2014). The increases in the C–S–H peak intensities of solidified samples compared to the unsolidified specimen are presented in Table 5. The improvement ratios based on the reflection intensity are highest for F10-C5, followed by F10-C20, and are lowest for C5.

The C–S–H peak intensities of C5 are lower than those of F10-C5 and F20-C5, confirming that the C–S–H products of C5 were induced from only the cement hydration reaction because of the lack of SiO_2 in fly ash. In contrast, the C–S–H peak intensities of F10-C5 are greater than those of C5 because additional C–S–H products were created by pozzolanic reactions. The 10% fly ash exhibited appropriate

amounts between $Ca(OH)_2$ (from the cement hydration reaction) and SiO_2 (from fly ash), providing the best C–S–H contents during the pozzolanic response. However, the C–S–H peak intensities of F20-C5 are smaller than those of F10-C5, indicating unsuitable proportions of $Ca(OH)_2$ and SiO_2 . Therefore, the strengths and moduli of the solidified sediments are highest for F10-C5, followed by F10-C20, and are lowest for C5, as discussed in “Destructive properties” The relationships between the average C–S–H peak intensity and q_u and q_t based on three reference reflections are illustrated in Fig. 10c, which can be expressed using exponential growth equations. The increases in q_u and q_t significantly depend on the C–S–H amounts.

Thermogravimetric analyzer

The relationship between the percentage of mass loss (m) versus the temperature (T) obtained from the TGA results for C5, F10-C5, and F20-C5 after curing periods of 28 and 120 days are presented in Fig. 11a and b, respectively. Significant mass losses are clearly observed for C–S–H products (primary m between 50 and 200 °C), calcium aluminum hydrate (CAH), and CASH (primary m between 200 and 300 °C) (Haha et al. 2011). The m increase is produced by releasing CO_2 and CaO induced by decomposing the unreacted hydrated calcium carbonate (Jiang et al. 2016; Sharma et al. 2012). The C–S–H and CAH/CASH contents in F10-C5 are higher than those in C5 and F20-C5, indicating a higher pozzolanic interaction. The correlations between m and q_u and q_t are presented in Fig. 11b. The m appeared to be a direct function of the behavior’s strength, which can be modeled as an exponential growth function.

Energy-dispersive X-ray analysis

Figure 12a and b show the EDX analysis results of the C5, F10-C5, and F20-C5 samples at curing periods of 28 and 120 days, respectively. Primary elements included silicon (Si), aluminum (Al), and calcium (Ca) (Jamsawang et al. 2017a; Tongwei et al. 2014; Wang et al. 2013). The amounts of Al, Si, and Ca in F10-C5 are higher than those in C5 and F20-C5. Ca and Si’s presence indicates appropriate conditions for forming C–S–H gels (Al-Homidy et al. 2017; Bilondi et al. 2018; Li and Poon 2017). This characteristic reveals that F10-C5 exhibited the best C–S–H gel formation and highest bond strength. These results confirm the finding of the highest strengths and moduli for solidified sediment with fly ash–cement blend at an optimal fly ash content of 10% in “Destructive properties” The correlations of q_u versus Ca content and q_t versus Ca content are presented in Fig. 8, which can be expressed using a modified power equation. The strength generally increased in proportion with the Ca content. The correlations obtained from the

Fig. 9 **a** Generalized strength development, **b** generalized modulus development, and **c** generalized strain at failure development for the solidified sediment

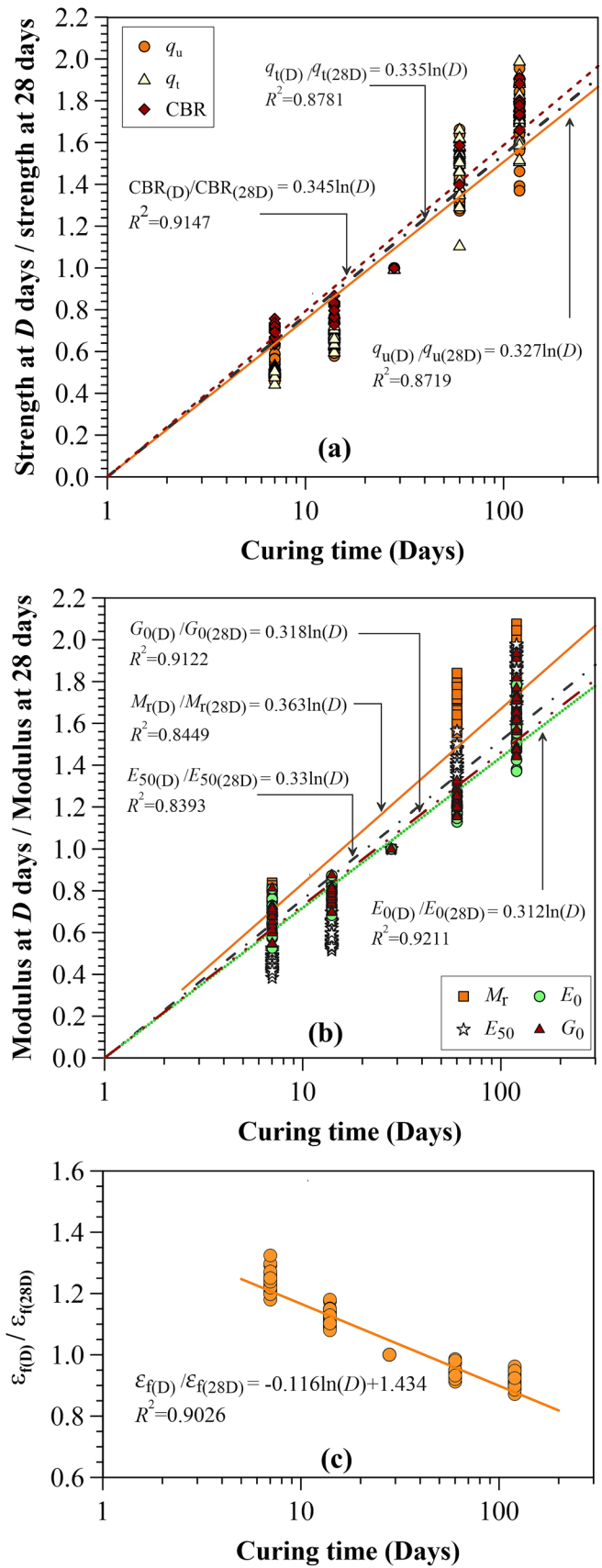


Fig. 10 XRD diffraction patterns of the solidified sediments at **a** 28 days and **b** 120 days, and **c** the relationship between the strength and CSH content

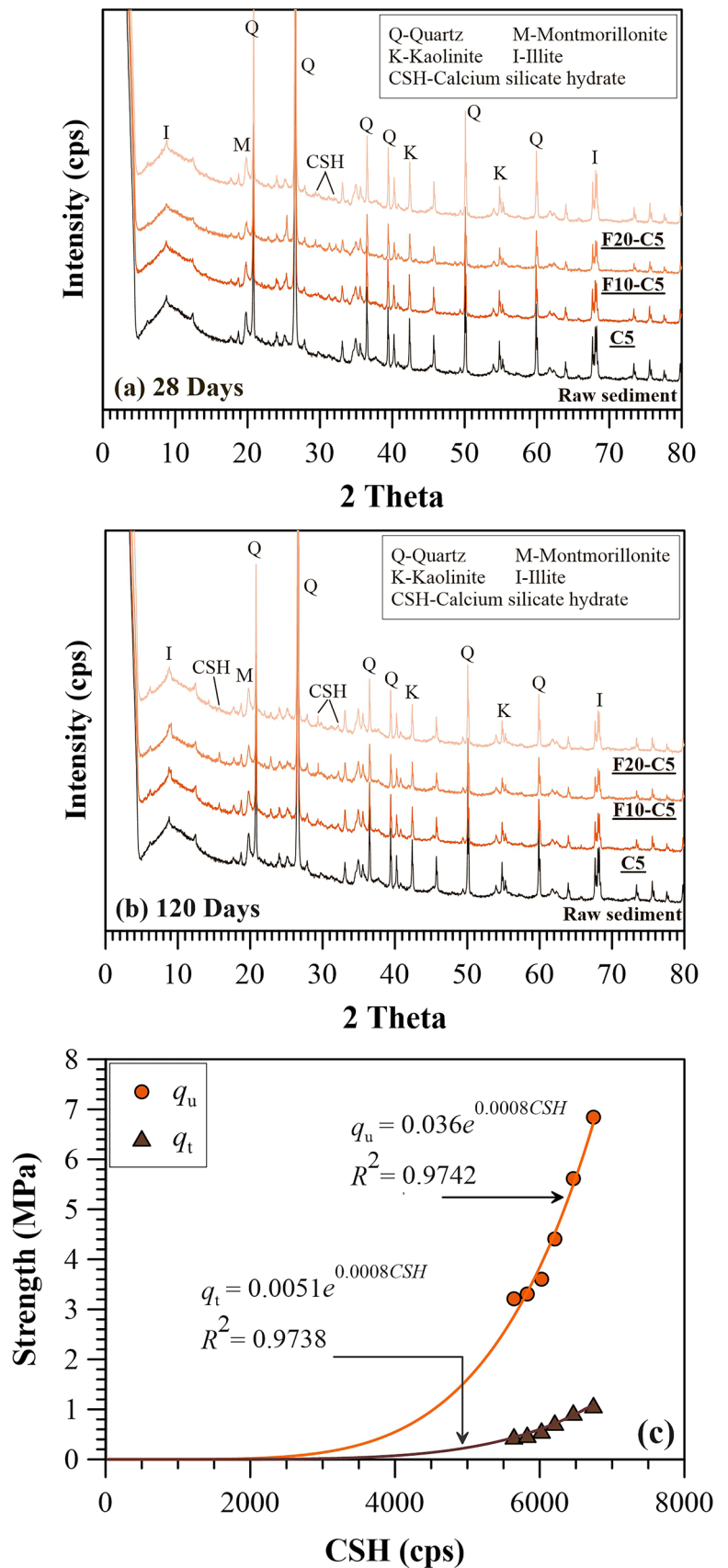


Table 5 Influence of fly ash-blended cement solidification on C-S-H peak intensities

Symbol	CSH at 28 days			Improvement ratio based on peak intensity		
	Reference peak at			Reference peak at		
	2 θ = 15.10°	2 θ = 29.80°	2 θ = 32.16°	2 θ = 15.10°	2 θ = 29.80°	2 θ = 32.16°
Unsolidified	7199	5529	5439	1.000	1.000	1.000
C5	7425	6209	6022	1.031	1.123	1.107
F10-C5	7766	6631	6219	1.079	1.199	1.143
F20-C5	7692	6412	5916	1.069	1.160	1.088

Symbol	CSH at 120 days			Improvement ratio based on peak intensity		
	Reference peak at			Reference peak at		
	2 θ = 15.10°	2 θ = 29.80°	2 θ = 32.16°	2 θ = 15.10°	2 θ = 29.80°	2 θ = 32.16°
Unsolidified	7199	5529	5439	1.000	1.000	1.000
C5	7982	6674	6473	1.109	1.207	1.190
F10-C5	8348	7128	6685	1.160	1.289	1.229
F20-C5	8269	6892	6359	1.149	1.247	1.169

microstructural analyses show that $q_t \approx 0.16q_u$, which indicated that the destructive and microstructural experiments provide similar results.

Scanning electron microscopy

SEM was used to study the microstructure of the mixtures to determine the particulate morphology at select sampling points. Sampling was performed at the failure surface of UC test samples of each mix because such surfaces can accurately represent any local specificities in physicochemical characteristics within the region of interest. At least three points on the failure surface were selected for SEM analysis. The magnification of the SEM micrographs used in this study is 3500 \times .

Figure 13 illustrates the microstructural morphologies of specimens C5, F10-C5, and F20-C5. After a curing period of 28 days, the cement hydration products, e.g., C-S-H gels, were detected in C5, and rough surfaces of the sample were clearly noted, but some voids between sediment particles were also observed (Jamsawang et al. 2017a; Yoobanpot et al. 2017, 2018). After a curing period of 120 days, the additional C-S-H gels derived from the pozzolanic reaction were created. The C-S-H products filled the voids between sediment particles and formed a framework on the sediment aggregates. This C-S-H formation pattern contributes to densifying the sediment aggregates and enhancing interparticle bonds, increasing the overall strength.

The SEM images of F10-C5 and F20-C5 reveal three forms of fly ash particles: particles with a disintegrated surface, a smooth surface, and a covering surface with the C-S-H products. The first form represented reacted fly ash particles with $\text{Ca}(\text{OH})_2$ in the pozzolanic reaction, creating

additional C-S-H gels (Chindaprasirt et al. 2007; Yoobanpot et al. 2017). The second form showed unreacted fly ash particles, acting as filler materials to fill voids in the sediment aggregates. The third form indicated the presence of chemical reaction products surrounding the fly ash particles. The fly ash particles with smooth surfaces and with covering surfaces with the hydration products were spotted in the SEM images of F10-C5 and F20-C5 at 28 days of curing. The fly ash particles spread in the C-S-H framework and filled the voids, decreasing the porosity of the whole specimen.

The SEM photos of F10-C5 at a curing time of 120 days illustrate the fly ash particles with disintegrated surfaces and fully developed covering surfaces of C-S-H products derived from hydration and pozzolanic reactions. This configuration indicates a high level of hydration and pozzolanic responses. A hydration gel crust was routinely created as the curing period increased, tightly connecting sediment and adjacent fly ash particles. The C-S-H products filled the specimen pore voids, resulting in the integration and connection of sediment particles. Thus, the solidified samples exhibited smaller pores and denser microstructures than the unsolidified sediments (Fig. 1). Thus, the integration and connection of the solidified samples detected at the microscale improved the destructive and nondestructive properties of the unsolidified sediments at the macroscale (Kang et al. 2014).

The SEM photos for F20-C5 indicate that the fly ash particles were partly encased by C-S-H shells; some fly ash particles had smooth surfaces. These characteristics indicated that the hydration and pozzolanic reaction levels of F20-C5 were lower than those of F10-C5. The decrease in the number of pores in the solidified samples with curing time was induced by the development of C-S-H products,

Fig. 11 TGA analysis results for **a** C5, **b** F10-C5, and **c** F20-C5 at 28 days and 120 days, and **d** relationships between the strengths and mass loss

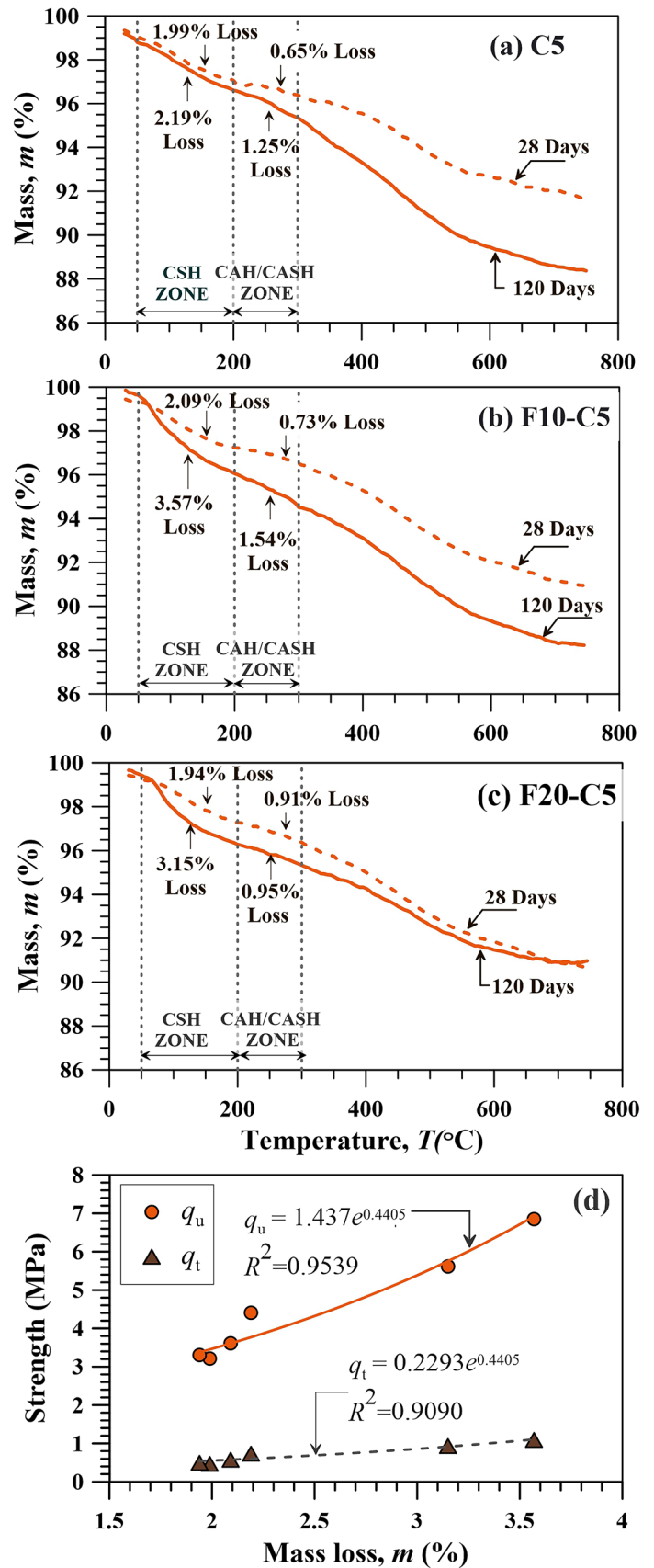
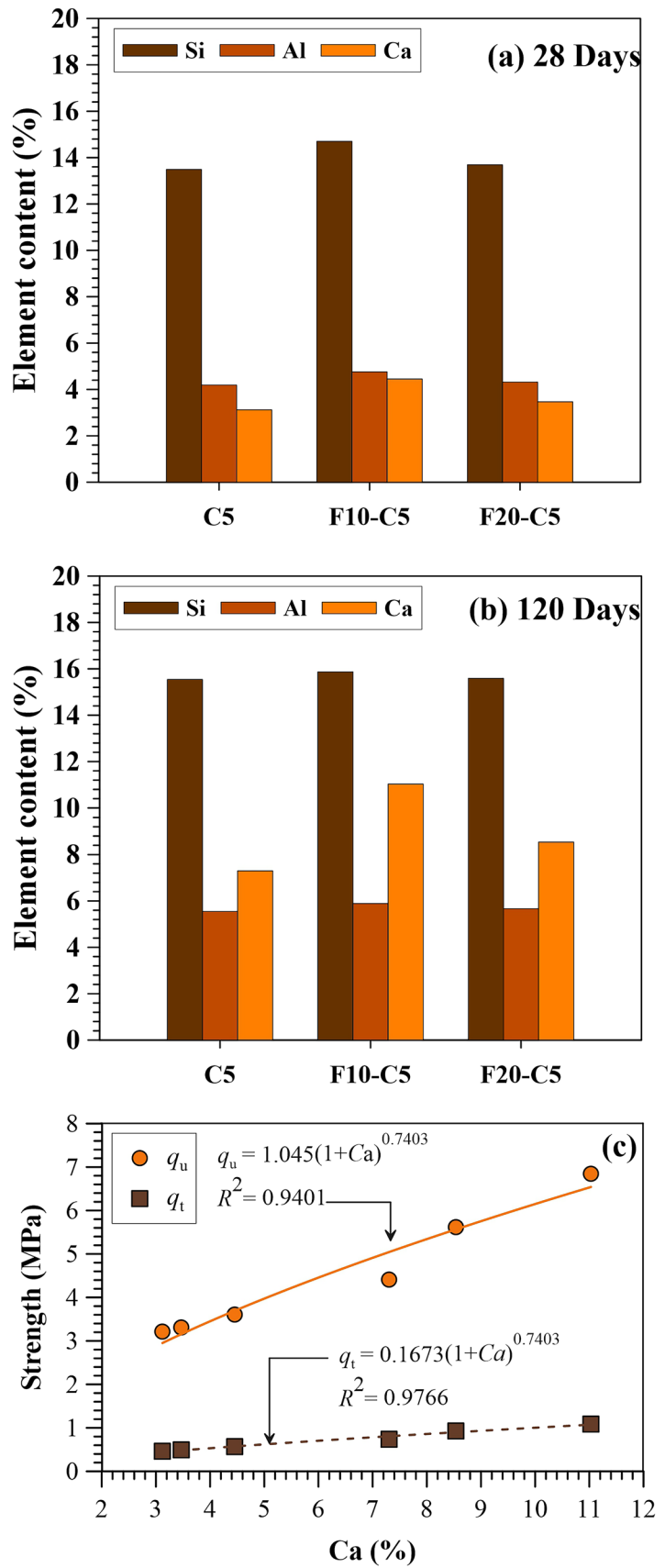


Fig. 12 EDX analysis results for C5, F10-C5, and F20-C5 C5-FA0 at **a** 28 days and **b** 120 days, and **c** the relationship between the strengths and Ca content



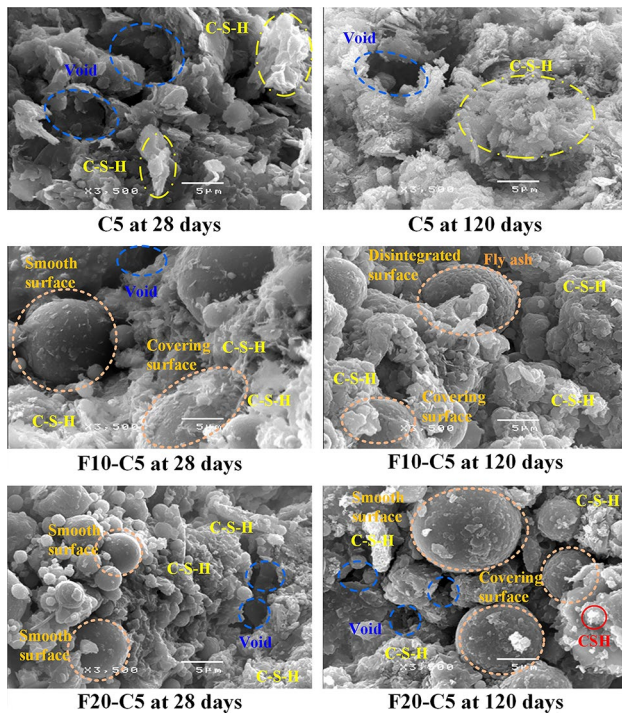


Fig. 13 SEM images with 3500 times magnification for samples C5, F10-C5, and F20-C5 at 28 days and 120 days

which caused increased internal bonds and filling of the void spaces between sediment particles (Yoobanpot et al. 2018). This phenomenon is the primary basis for destructive and nondestructive property developments, as discussed in Sects. 3.1 and 3.2. An enormous amount of C-S-H products was detected in F10-C5, followed by F20-C5 and C5. In contrast, the smallest pores were also observed in F10-C5, followed by F20-C5 and C5, for the described reasons. The SEM results proved that 10% fly ash–cement blend exhibited the most significant strengths and moduli and the lowest porosity (Jamsawang et al. 2017a).

Proposed strength prediction model

Based on microstructural analysis results, parameters affecting the $q_{u,D}$ of the solidified sediment with fly ash-blended cement samples included C-S-H peak intensity, mass loss (m), Ca amount, and D (curing period). All influencing factors showed nonlinear correlations with the q_u values of the solidified sediments. General multiple linear regression analyses were performed to integrate these parameters. Multiple linear regression, also known simply as multiple regression, is a statistical technique that uses several explanatory variables to predict the outcome of a response variable. Multiple linear regression aims to model the linear relationship between the explanatory (independent) variables and response (dependent) variables. The formula for multiple linear regression is:

$$y = \beta_0 + \beta_1 x_1 + \dots + \beta_n x_n + \epsilon \quad (3)$$

where:

-
- y = the predicted value of the dependent variable
 - x_1 = the first independent variable
 - x_2 = the last independent variable
 - β_0 = the y-intercept (value of y when all other parameters are set to zero)
 - β_1 = the regression coefficient of the first independent variable
 - β_n = the regression coefficient of the last independent variable
 - ϵ = model error
-

In multiple linear regression, three calculations are carried out to determine the best-fit line for each independent variable, including (1) the regression coefficients leading to the smallest overall model error, (2) the t -statistic of the overall model, and (3) the associated p -value. Then, the t -statistic and p -value are determined for each regression coefficient in the model. The regression results for reservoir sediment solidified with 0–20% fly ash blended with 5% cement are as follows:

$$q_{u,D} = 0.3889(Ca) - 0.0005098(C - S - H) + 0.903(m) - 0.003814(D) + 3.2146 \quad (4)$$

where $q_{u,D}$ is the solidified sediment's strength with cement blend FA after D days of curing time. A comparison between the experimental observation and predicted values obtained from Eq. 4 is presented in Fig. 14. The observed $q_{u,D}$ was very close to the proposed predicted $q_{u,D}$, with $R^2 = 0.9993$. The absolute error percentages of the $q_{u,D}$ values were 0.8–2% and 0.07–0.19% for the curing periods of 28 and 120 days, respectively. The error for samples subjected to a short period was more significant than that for specimens under a long period since the short-term strengths of solidified samples were unstable and changed significantly among samples. This finding is in contrast to that of the long-term strengths, which developed consistently, reducing the associated prediction error of the model.

Role of fly ash in the cement stabilization mechanism

Using fly ash-blended cement was more effective than using sole cement or sole fly ash because of the tremendous amounts of C-S-H produced by both hydration and pozzolanic reactions owing to the presence of SiO_2 in fly ash. Employing sole cement creates C-S-H from the hydration reaction because of the absence of SiO_2 from the fly ash. Utilizing fly ash alone is the least effective approach due to the lack of CaO from cement, which caused the lowest CSH amounts. In this study, a fly ash content of 10% was verified as the most effective because it delivered the best strengths

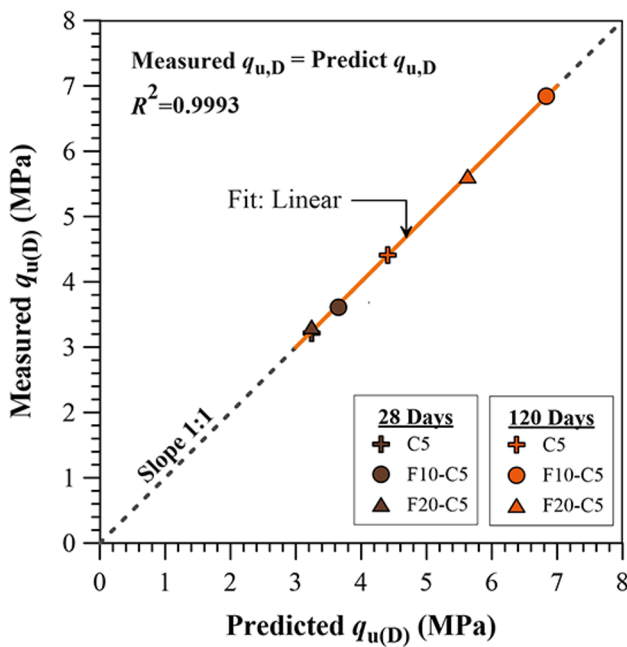


Fig. 14 Comparisons between the measured and predicted $q_{u(D)}$ values based on multiple regression analysis

and moduli of the solidified sediments for all cement contents and curing periods. This content provided the most appropriate SiO_2 and $CaOH_2$ proportions to create the most extensive C-S-H products. Excess fly ash contents of 10% caused decreases in strengths and moduli. They blocked the cement grains and prevented the interaction between the cement and water, reducing the hydration reaction level and reducing the C-S-H products.

Conclusions

This work exhibits the destructive and nondestructive properties and microstructural characteristics of reservoir sediments solidified with a fly ash–cement blend. The raw sediment, which was classified as well-graded sand with silt, was stabilized with class C fly ash and type I ordinary Portland cement. Fly ash (5–20%) and cement (1.5–5%) by weight of dry sediment were mixed to improve the mechanical properties of the mixtures. Based on the destructive and nondestructive test results as well as microstructural characteristics, the following conclusions can be drawn:

1. The evolution of the destructive and nondestructive properties of the solidified sediments was similar for all mix proportions. The use of fly ash alone can improve the q_u values approximately 1.25–3.76 times greater than those of the unsolidified sediments. Exclusive cement and fly ash–cement blend can enhance the q_u values by approximately 1.84–9.13 and 1.38–8.43 times, respectively, relative to unsolidified sediments.

2. The ϵ_f and ν_0 values for the solidified sediments ranged from 2–3.2% and 0.255–0.346, respectively. High q_u values caused an increase in the brittleness level of the solidified samples, resulting in decreasing ϵ_f . However, the relationship between ν_0 and q_u was independent. ν_0 depended on the property of the natural sediment rather than that of the solidified sediments.
3. The q_u of the solidified sediments was used as a primary indicator to create the linear empirical relationships, which can be quickly utilized for estimating the other destructive and nondestructive properties. Relations of $E_{50} = 81q_u$, $M_r = 151q_u$, $E_0 = 33q_u$, and $G_0 = 10q_u$ for the solidified sediment were obtained in the current study.
4. The durability of solidified samples against WDC depended on the initial q_u . Using 6 WDCs is sufficient for solidified sediments because of the lower $q_{u(WDC)}$ than the given values. The correlation between the strength and the number of WDCs can be utilized to evaluate the pavement lifetime using solidified sediments as road materials.
5. All microstructural analysis results prove that F10-C5 provided the best C-S-H contents compared to F20-C5 and C5, through various interpretations. The XRD and TGA results found the highest C-S-H peak intensities and maximum mass losses in F10-C5, respectively. The EDX analyses indicated the most significant weight proportion of Ca for F10-C5. The SEM images illustrate the enormous amounts of C-S-H products. The microscale findings confirm that the 10% fly ash–cement blend exhibited the best destructive and nondestructive characteristics at the macroscale.

Acknowledgements This project was funded by King Mongkut’s University of Technology North Bangkok and the National Research Council of Thailand (NRCT) under contract no.NRCT5-RSA63007-01. Pornkasem Jongpradist The fourth author (P. Jongpradist) appreciates the financial support provided by the National Research Council of Thailand (NRCT) through Thailand Science Research and Innovation (TSRI) under Fundamental Fund 2022 (Project: Advanced Construction Towards Thailand 4.0). The fourth author (S.Likitlersuang) would like to acknowledge the Thailand Science Research and Innovation Fund Chulalongkorn University (CU_FRB65_dis(28)_143_21_09).

Declarations

Ethics approval and consent to participate The authors state that the research was conducted according to ethical standards.

Conflict of interest The authors declare no competing interests.

References

AASHTO (2012) Standard method of test for determining the resilient modulus of soils and aggregate materials T 307. Washington, DC
 Agapitus AA (2014) Enhancing durability of quarry fines modified black cotton soil subgrade with cement kiln dust stabilization. *Transport Geotech* 1:55–61

- Aldaood A, Bouasker M, Al-Mukhtar M (2014) Impact of wetting–drying cycles on the microstructure and mechanical properties of lime-stabilized gypseous soils. *Eng Geol* 174:11–21
- Al-Homidy AA, Dahim MH (2017) Abd El Aal AK, Improvement of geotechnical properties of sabkha soil utilizing cement kiln dust. *J Rock Mech Geotech Eng* 9(4):749–760
- Al-Mukhtar M, Lasledj A, Alcover J-F (2010a) Behaviour and mineralogy changes in lime-treated expansive soil at 50°C. *Appl Clay Sci* 50(2):199–203
- Al-Mukhtar M, Lasledj A, Alcover J-F (2010b) Behaviour and mineralogy changes in lime-treated expansive soil at 20°C. *Appl Clay Sci* 50(2):191–198
- Ardah A, Chen Q, Abu-Farsakh M (2017) Evaluating the performance of very weak subgrade soils treated/stabilized with cementitious materials for sustainable pavements. *Transp Geotech* 11:107–119
- Arora S, Aydilek AH (2005) Class F fly-ash-amended soils as highway base materials. *J Mater Civ Eng* 17(6):640–649
- ASTM (2016a) Standard test method for unconfined compressive strength of cohesive soil D 2166/D 2166M. West Conshohocken, PA: ASTM International
- ASTM (2016b) Standard test method for splitting tensile strength of intact rock core D 3967. West Conshohocken, PA: ASTM International
- ASTM (2016c) Standard test method for California bearing ratio (CBR) of laboratory-compacted soil D 1883. West Conshohocken, PA: ASTM International
- ASTM (2015) Standard test methods for wetting and drying compacted soil-cement mixtures D559. West Conshohocken, PA: ASTM International
- ASTM (2019) Standard test method for fundamental transverse, longitudinal, and torsional resonant frequencies of concrete specimens C215. West Conshohocken, PA: ASTM International
- Austrroads (2017) Guide to pavement technology Part 2: Pavement structural design. Austrroads, Sydney
- Baldovino JA, Moreira EB, Izzo RLS, Rose JL (2018) Empirical relationships with unconfined compressive strength and split tensile strength for the long term of a lime-treated silty soil. *J Mater Civ Eng* 30(8):06018008
- Banoune B, Melbouci B, Rosquoe F, Langlet T (2016) Treatment of river sediments by hydraulic binders for valorization in road construction. *Bull Eng Geol Environ* 75:1505–1517
- Bilondi MP, Toufigh MM, Toufigh V (2018) Experimental investigation of using a recycled glass powder-based geopolymer to improve the mechanical behavior of clay soils. *Constr Build Mater* 170:302–313
- Biswal DR, Sahoo UC, Dash SR (2020) Non-destructive strength and stiffness evaluation of cement-stabilised granular lateritic soils. *Road Mater Pavement Des* 21(3):835–849
- Bogas JA, Gomes MG, Gomes A (2013) Compressive strength evaluation of structural lightweight concrete by non-destructive ultrasonic pulse velocity method. *Ultrasonics* 53(5):962–672
- Bowles JE (1997) Foundation analysis and design, 5th Edition. McGraw–Hill
- Chan CM (2016) Geo-parametric study of dredged marine clay with solidification for potential reuse as good engineering soil. *Environ Earth Sci* 75(11):1–15
- Chindapasirt P, Jaturapitakkul C, Sinsiri T (2007) Effect of fly ash fineness on microstructure of blended cement paste. *Constr Build Mater* 21:1534–1541
- Chompoorat T, Maikhun T, Likitlersuang S (2019) Cement improved lake bed sedimentary soil for road construction. *Proceedings of the Institution of Civil Engineers – Ground Improvement* 172(3):192–201
- Chompoorat T, Likitlersuang S, Sitthiawiruth S, Komolvilas V, Jamsawang P, Jongpradist P (2021a) Mechanical properties and microstructures of stabilised dredged expansive soil from coal mine. *Geomechanics and Engineering* 25(2):143–157
- Chompoorat T, Likitlersuang S, Thepumong T, Tanapalungkorn W, Jamsawang P, Jongpradist P (2021b) Solidification of sediments deposited in reservoirs with cement and fly ash for road construction. *Int J Geosynthet Ground Eng* 7(4):85
- Chompoorat T, Thepumong T, Khamplod A, Likitlersuang S (2022) Improving mechanical properties and shrinkage cracking characteristics of soft clay in deep soil mixing. *Constr Build Mater* 316:125858
- Consoli NC, da Rocha CG, Silvani C (2014) Effect of curing temperature on the strength of sand, coal fly ash, and lime blends. *J Mater Civ Eng* 26(8):06014015
- Dang TA, Kamali-Bernard S, Prince WA (2013) Design of new blended cement based on marine dredged sediment. *Constr Build Mater* 41:602–611
- Dubois V, Zentar R, Abriak NE, Grégoire P (2011) Fine sediments as a granular source for civil engineering. *Eur J Environ Civ Eng* 15:137–166
- Furlan AP, Razakamanantsoa A, Ranaivomanana H, Levacher D, Katsumi T (2018) Shear strength performance of marine sediments stabilized using cement, lime and fly ash. *Constr Build Mater* 184:454–463
- Guimond-Barrett A, Nauleau E, LeKouby A, Pantet A, Reiffsteck P (2013) Free–free resonance testing of in situ deep mixed soils. *Geotechn Test J* 36(2):283–291
- Güllü H, Canakci H, Zangana IFA (2017) Use of cement based grout with glass powder for deep mixing. *Constr Build Mater* 137:12–20
- Haha MB, Lothenbach B, Saout GL, Winnefeld F (2011) Influence of slag chemistry on the hydration of alkali-activated blast-furnace slag – Part I: Effect of MgO. *Cem Concr Res* 41(9):955–963
- Horpibulsuk S, Phetchuay C, Chinkulkijniwat A, Cholaphatsorn A (2013) Strength development in silty clay stabilized with calcium carbide residue and fly ash. *Soils Found* 53(4):477–486
- Horpibulsuk S, Phojan W, Suddeepong A, Chinkulkijniwat A, Liu MD (2012) Strength development in blended cement admixed saline clay. *Appl Clay Sci* 55:44–52
- Horpibulsuk S, Rachan R, Chinkulkijniwat A, Raksachon Y (2010) Analysis of strength development in cement-stabilized silty clay from microstructural considerations. *Constr Build Mater* 24(10):2011–2021
- Horpibulsuk S, Rachan R, Raksachon Y (2009) Role of fly ash on strength and microstructure development in blended cement stabilized silty clay. *Soils Found* 49(1):85–98
- Horpibulsuk S, Rachan R, Suddeepong A (2011a) Assessment of strength development in blended cement admixed Bangkok clay. *Constr Build Mater* 25(4):1521–1531
- Horpibulsuk S, Rachan R, Suddeepong A, Chinkulkijniwat A (2011b) Strength development in cement admixed Bangkok clay: laboratory and field investigations. *Soil Found* 51(2):239–251
- Jamsawang P, Nuansrithong N, Voottipruex P, Songpiriyakij S, Jongpradist P (2017a) Laboratory investigations on the swelling behavior of composite expansive clays stabilized with shallow and deep clay-cement mixing methods. *Appl Clay Sci* 148:83–94
- Jamsawang P, Poorahong H, Yoobanpot N, Songpiriyakij S, Jongpradist P (2017b) Improvement of soft clay with cement and bagasse ash waste. *Constr Build Mater* 154:61–71
- Jamsawang P, Suansomjeen T, Sukontasukkul P, Jongpradist P, Bergado DT (2018) Comparative flexural performance of compacted cement-fiber-sand. *Geotext Geomembr* 46(4):414–425
- Jamsawang P, Voottipruex P, Horpibulsuk S (2015) Flexural strength characteristics of compacted cement-polypropylene fiber sand. *J Mater Civ Eng* 27(9):04014243
- Jamsawang P, Charoensil S, Jongpradist P, Likitlersuang S (2021) Mechanical and microstructural properties of dredged sediments

- treated with cement and fly ash for use as pavement materials. *Road Materials and Pavement Design* 22(11):2498–2522
- Jiang N, Du Y, Liu S, Wei M, Horpibulsuk S, Arulrajah A (2016) Multi-scale laboratory evaluation of the physical, mechanical, and microstructural properties of soft highway subgrade soil stabilized with calcium carbide residue. *Can Geotech J* 53(3):373–383
- Jiang NJ, Du YJ, Liu K (2018) Durability of lightweight alkali-activated ground granulated blast furnace slag (GGBS) stabilized clayey soils subjected to sulfate attack. *Appl Clay Sci* 161:70–75
- Kamali S, Bernard F, Abriak NE (2008) Marine dredged sediments as new materials resource for road construction. *Waste Manage* 28:918–928
- Kampala A, Horpibulsuk S (2013) Engineering properties of silty clay stabilized with calcium carbide residue. *J Mater Civ Eng* 25(5):632–644
- Kampala A, Horpibulsuk S, Prongmanee N, Chinkulkijniwat A (2014) Influence of wet-dry cycles on compressive strength of calcium carbide residue-fly ash stabilized clay. *J Mater Civ Eng* 26(4):633–643
- Kang X, Kang G-C, Chang K-T, Ge L (2014) Chemically stabilized soft clays for road-base construction. *J Mater Civ Eng* 27(7):04014199
- Kolias S, Kasselouri-Rigopoulou V, Karahalios A (2005) Stabilization of clayey soil with high calcium fly ash cement. *Cem Concr Compos* 27:301–313
- Larsson S (2005) State of practice report—execution, monitoring and quality control. *Proceedings of the International Conference on Deep Mixing Best Practice and Recent Advances*, Stockholm, Sweden 2:732–786
- Li J, Poon CS (2017) Innovative solidification/stabilization of lead contaminated soil using incineration sewage sludge ash. *Chemosphere* 173:143–152
- Mamatha KH, Dinesh SV (2017) Resilient modulus of black cotton soil. *Int J Pavement Res Technol* 10(2):171–184
- Meei-Hoan H, Chee-Ming C (2014) The potential of using rubber-chips as a soft clay stabilizer enhancing agent. *Mod Appl Sci* 4(10):122–131
- Mohammadinia A, Arulrajah A, Sanjayan J, Disfani MM, Bo MW, Darmawan S (2015) Laboratory evaluation of the use of cement-treated construction and demolition materials in pavement base and subbase applications. *J Mater Civ Eng* 27:04014186-1–4014210
- Moon SW, Vinoth G, Subramanian S, Kim J, Ku T (2020) Effect of fine particles on strength and stiffness of cement treated sand. *Granular Matter* 22(9):1–13
- Mutaz E, Dafalla MA (2014) Chemical analysis and X-ray diffraction assessment of stabilized expansive soils. *Bull Eng Geol Environ* 73:1063–1072
- Nazarian S, Yuan D, Tandon V (1999) Structural field testing of flexible pavement layers with seismic methods for quality control. *Transp Res Rec* 1654(1):50–60
- Portland Cement Association (PCA) (1992) *Soil-cement laboratory handbook*. Portland Cement Association, Skokie, IL
- Ryden N, Ekdahl U, Lindh P (2006) Quality control of cement stabilized soils using non-destructive seismic tests. *Proc Adv Test Fresh Cem Mater* 34:295–300
- Sharma NK, Swain SK, Sahoo UC (2012) Stabilization of a clayey soil with fly ash and lime: a micro level investigation. *Geotech Geol Eng* 30(5):1197–1205
- Shon C-S, Saylak D, Mishra SK (2010) Combined use of calcium chloride and fly ash in road base stabilization. *Transp Res Rec* 2186(1):120–129
- Silitonga E, Levacher D, Mezazigh S (2009) Effects of the use of fly ash as a binder on the mechanical behaviour of treated dredged sediments. *Environ Technol* 30(8):799–807
- Silitonga E, Levacher D, Mezazigh S (2010) Utilization of fly ash for stabilization of marine dredged sediments. *Eur J Environ Civ Eng* 14(2):253–265
- Tang CS, Cui YJ, Shi B, Tang AM, Liu C (2011) Desiccation and cracking behaviour of clay layer from slurry state under wetting-drying cycles. *Geoderma* 166:111–118
- Tastan EO, Edil TB, Benson CH, Aydilek AH (2011) Stabilization of organic soils with fly ash. *J Geotech Geoenviron Eng* 137(9):819–833
- Tongwei Z, Xibing Y, Yongfeng D, Dingwen Z, Songyu L (2014) Mechanical behaviour and micro-structure of cement-stabilised marine clay with a metakaolin agent. *Constr Build Mater* 73:51–57
- Tripathy S, Rao SSK (2009) Cyclic swell-shrink behavior of a compacted expansive soil. *Geotech Geol Eng J* 27(1):89–103
- U.S. Army Corps of Engineers (COE) (2004) *Soil stabilization for pavements*. TM 5-822-14/AFJMAN 32/1019
- Verástegui-Flores RD, Emidio GD, Bezuijen A, Vanwalleghem J, Kersemans M (2015) Evaluation of the free-free resonant frequency method to determine stiffness moduli of cement-treated soil. *Soils Found* 55(5):943–950
- Voottipruex P, Jamsawang P (2014) Characteristics of expansive soils improved with cement and fly ash in Northern Thailand. *Geomech Eng* 6:437–453
- Wang D, Abriak NE, Zentar R (2013) Strength and deformation properties of Dunkirk marine sediments solidified with cement, lime and fly ash. *Eng Geol* 166:90–99
- Wang D, Abriak NE, Zentar R, Xu WY (2012) Solidification / stabilization of dredged marine sediments for road construction. *Environ Technol* 33(1):95–101
- Wang D, Zentar R, Abriak NE (2018) Durability and swelling of solidified / stabilized dredged marine soils with class-F fly ash, cement, and lime. *30(3):04018013*
- Yesiller N, Hanson JL, Usmen M (2001) Ultrasonic assessment of stabilized soils. *Proc ASCE Geo-Institute Soft Gr Technol Conf* 170–181
- Yoobanpot N, Jamsawang P, Horpibulsuk S (2017) Strength behavior and microstructural characteristics of soft clay stabilized with cement kiln dust and fly ash residue. *Appl Clay Sci* 141:146–156
- Yoobanpot N, Jamsawang P, Krairan K, Jongpradist P, Horpibulsuk S (2018) Reuse of dredged sediments as pavement materials by cement kiln dust and lime treatment. *Geotech Eng* 15(4):1055–1016
- Yoobanpot N, Jamsawang P, Poorahong H, Jongpradist P, Likitlersuang S (2020a) Multiscale laboratory investigation of the mechanical and microstructural properties of dredged sediments stabilized with cement and fly ash. *Eng Geol* 267:105491
- Yoobanpot N, Jamsawang P, Simarat P, Jongpradist P, Likitlersuang S (2020b) Sustainable reuse of dredged sediments as pavement materials by cement and fly ash stabilization. *J Soils Sediments* 20(10):3807–3823
- Zeng LL, Hong ZS, Gao YF (2017) Practical estimation of compression behaviour of dredged clays with three physical parameters. *Eng Geol* 217:102–109
- Zentar R, Wang H, Wang D (2021) Comparative study of stabilization / solidification of dredged sediments with ordinary Portland cement and calcium sulfo-aluminate cement in the framework of valorization in road construction material. *Constr Build Mater* 279:122447
- Zhang W, McCabe BA, Chen Y, Forkan TJ (2018) Unsaturated behaviour of a stabilized marine sediment: A comparison of cement and GGBS binders. *Eng Geol* 246:57–68